Brain, Behavior, and Immunity 110 (2023) 348–364

Contents lists available at ScienceDirect

Brain Behavior and Immunity

journal homepage: www.elsevier.com/locate/ybrbi

Full-length Article

Schwann cell insulin-like growth factor receptor type-1 mediates metastatic bone cancer pain in mice

Lorenzo Landini [a,1], Matilde Marini [a,1], Daniel Souza Monteiro de Araujo [a,1], Antonia Romitelli [a], Marco Montini [b], Valentina Albanese [c], Mustafa Titiz [a], Alessandro Innocenti [d], Francesca Bianchini [e], Pierangelo Geppetti [a], Romina Nassini [a,*], Francesco De Logu [a]

[a] Department of Health Sciences, Clinical Pharmacology and Oncology Section, University of Florence, Florence 50139, Italy
[b] Department of Experimental and Clinical Biomedical Sciences "Mario Serio", Medical Genetics Unit, University of Florence, 50141 Florence, Italy
[c] Department of Environmental and Prevention Sciences - DEPS, University of Ferrara, Ferrara 44121, Italy
[d] Plastic and Reconstructive Microsurgery - Careggi University Hospital, Florence 50139, Italy
[e] Department of Experimental and Clinical Biomedical Sciences "Mario Serio", Section of Experimental Pathology and Oncology, University of Florence, 50141 Florence, Italy

ARTICLE INFO

Keywords:
Bone cancer pain
Osteoclast derived IGF-1
Schwann cells
TRPA1
Oxidative stress

ABSTRACT

Insulin growth factor-1 (IGF-1), an osteoclast-dependent osteolysis biomarker, contributes to metastatic bone cancer pain (MBCP), but the underlying mechanism is poorly understood. In mice, the femur metastasis caused by intramammary inoculation of breast cancer cells resulted in IGF-1 increase in femur and sciatic nerve, and IGF-1-dependent stimulus/non-stimulus-evoked pain-like behaviors. Adeno-associated virus-based shRNA selective silencing of IGF-1 receptor (IGF-1R) in Schwann cells, but not in dorsal root ganglion (DRG) neurons, attenuated pain-like behaviors. Intraplantar IGF-1 evoked acute nociception and mechanical/cold allodynia, which were reduced by selective IGF-1R silencing in DRG neurons and Schwann cells, respectively. Schwann cell IGF-1R signaling promoted an endothelial nitric oxide synthase-mediated transient receptor potential ankyrin 1 (TRPA1) activation and release of reactive oxygen species that, *via* macrophage-colony stimulating factor-dependent endoneurial macrophage expansion, sustained pain-like behaviors. Osteoclast derived IGF-1 initiates a Schwann cell-dependent neuroinflammatory response that sustains a proalgesic pathway that provides new options for MBCP treatment.

1. Introduction

Pain is a recurrent symptom of cancer that becomes more frequent and debilitating in the presence of bone metastases, which is a common consequence of many primary tumors, including breast cancer (Rades et al., 2010). Treatment of metastatic bone cancer pain (MBCP) represents a major medical challenge, as current therapies are insufficient, resulting in psychological distress, anxiety, and significantly reduced quality of life (von Moos et al., 2017). The mechanism of MBCP involves several interactions between tumor and bone cells, activated inflammatory cells, and bone-innervating neurons (Andriessen et al., 2021; Zajaczkowska et al., 2019). Although bone resorption associated with the invasion of cancer cells has been considered as the primary cause of MBCP (Mantyh, 2006; Mantyh, 2014), knowledge of the cellular and molecular mechanisms underlying MBCP is limited.

Mediators produced by breast cancer cells that directly stimulate

Abbreviations: IGF-1, Insulin Growth Factor-1; MBCP, Metastatic Bone Cancer Pain; IGF-1R, IGF-1 receptor; TRPA1, Transient Receptor Potential Ankyrin 1; DRG, Dorsal Root Ganglion; IL, Interleukin; TNF, Tumor Necrosis Factor; FGF, Fibroblast Growth Factors; TGF, Transforming Growth Factor; BMP, Bone Morphogenetic Proteins; CNS, Central Nervous System; M-CSF, Macrophage-Colony Stimulating Factor; AAV, Adeno-Associated Virus; HSCs, Human Schwann cells; NO, Nitric Oxide; H_2O_2, Hydrogen Peroxide; PPP, Picropodophyllin; PBN, Phenyl-alpha-tert-Butyl Nitrone; IRS-1, Insulin Receptor Substrate 1; eNOS, endothelial Nitric Oxide Synthase; PKC, Protein Kinase C; CGRP, Calcitonin Gene-Related Peptide; MAFIA, Macrophages Fas-Induced Apoptosis.

* Corresponding author at: Department of Health Sciences, Section of Clinical Pharmacology and Oncology, University of Florence, Viale Pieraccini, 6, 50139 Florence, Italy.
E-mail address: romina.nassini@unifi.it (R. Nassini).
[1] These authors contributed equally to this work.

https://doi.org/10.1016/j.bbi.2023.03.013
Received 30 November 2022; Received in revised form 27 February 2023; Accepted 16 March 2023
Available online 20 March 2023

osteoclast activity comprise interleukin (IL)-8, IL-11, and tumor necrosis factor (TNF)-α (Le Pape et al., 2016; Weilbaecher et al., 2011). Osteoclasts activated in osteolytic lesions caused by metastatic growth are known to release several proinflammatory compounds and growth factors. These include IL-6 (Ara and Declerck, 2010), fibroblast growth factors (FGF) (Aukes et al., 2017), transforming growth factor (TGF)-β (Guise, 2000), bone morphogenetic proteins (BMP) (Katsuno et al., 2008), and insulin-like growth factor 1 (IGF-1) (Aielli et al., 2019). All these mediators may potentially contribute to the deterioration of the bone matrix and promote tumor cell proliferation and the growth of bone metastases (Fohr et al., 2003), and some may be directly or indirectly implicated in pain transmission (Echeverry et al., 2009; Forouzanfar and Sadeghnia, 2020; Mitchell et al., 2016; Zhang et al., 2014; Zhou et al., 2016). Initially, IGF-1 was reported to elicit analgesic activity in the central nervous system (CNS) (Bitar et al., 1996), and interference with IGF-1 signaling in microglia was found to impair pain recovery after peripheral nerve injury in mice (Kohno et al., 2022). However, it has long been known that IGF-1 subcutaneous administration in rodents induces local proalgesic responses (Miura et al., 2011; Zhang et al., 2014) that are thought to be mediated by activation of the tyrosine kinase IGF-1 receptor (IGF-1R) in dorsal root ganglion (DRG) neurons (Tang et al., 2019). Inhibition of IGF-1R was found to reduce the mechanical and thermal allodynia associated with bone cancer in rats (Li et al., 2014). However, the site and mechanism underlying the proalgesic action of IGF-1 are poorly understood.

A prominent role of Schwann cells in maintaining neuroinflammation in peripheral nerves and sustaining prolonged allodynia has recently been reported in various mouse models of neuropathic and cancer pain (De Logu et al., 2019; De Logu et al., 2021; De Logu et al., 2022; De Logu et al., 2017; Wang et al., 2022). An oxidative stress-dependent feed-forward pathway between macrophage-colony stimulating factor (M-CSF) and Schwann cells that sustains neuroinflammation and mechanical allodynia by amplifying the oxidative stress burden was reported in a mouse model of cancer pain (De Logu et al., 2021). We hypothesized that osteoclast-dependent osteolysis mediators target Schwann cells to elicit MBCP. To address this hypothesis, we used adeno-associated virus (AAV)-mediated cell-specific IGF-1R silencing in Schwann cells or DRG neurons in a mouse model of MBCP obtained by E0771 breast carcinoma cell inoculation into the mammary gland (Ewens et al., 2005; Hiraga and Ninomiya, 2019).

2. Materials and methods

2.1. Animals

Female mice were used throughout (25–30 g, 5–8 weeks old). The following strains of mice were used: C57BL/6 J (Charles River, RRID: IMSR_JAX:000664), wild-type (*Trpa1*$^{+/+}$), and TRPA1-deficient (*Trpa1*$^{-/-}$; B6129P-Trpa1^{tm1Kykw}/J; RRID: IMSR_JAX:006401, Jackson Laboratory) mice (Kwan et al., 2006). Genetically modified mice were maintained as heterozygotes on the C57BL/6 J background. To generate mice in which the Trpa1 gene was conditionally silenced in Schwann cells, homozygous 129S-Trpa1$^{tm2Kykw/J}$ (floxed Trpa1, *Trpa1*$^{fl/fl}$, RRID: IMSR_JAX: 008649 Jackson Laboratory) were crossed with hemizygous B6.Cg-Tg(Plp1-CreERT)3Pop/J mice (Plp-Cre^{ERT}, RRID: IMSR_JAX:005975 Jackson Laboratory) expressing a tamoxifen-inducible Cre in their Schwann cells (Plp1, proteolipid protein myelin 1) (De Logu et al., 2017). The progeny (Plp-Cre^{ERT}; *Trpa1*$^{fl/fl}$) was genotyped using PCR for Trpa1 and Plp-Cre^{ERT}. Mice that were negative for Plp1-Cre^{ERT} (Plp-Cre^{ERT-}; *Trpa1*$^{fl/fl}$) were used as controls. Both positive and negative mice for Cre^{ERT} and homozygous floxed Trpa1 (Plp-Cre^{ERT+}; *Trpa1*$^{fl/fl}$ and Plp-Cre^{ERT-}; *Trpa1*$^{fl/fl}$, respectively) were treated with i.p. 4-OHT (1 mg/100 μL in corn oil) once a day consecutively for 3 d. This treatment resulted in the Cre-mediated ablation of Trpa1 in Schwann cells expressing Plp. To selectively delete Trpa1 in primary sensory neurons, *Trpa1*$^{fl/fl}$ mice were crossed with hemizygous Advillin-Cre mice (Adv-Cre) (De Logu et al., 2017; Zurborg et al., 2011). Mice that were positive or negative for Cre and homozygous for floxed Trpa1 (Adv-Cre^{+}; *Trpa1*$^{fl/fl}$ and Adv-Cre^{-}; *Trpa1*$^{fl/fl}$, respectively) were used. The successful Cre-driven deletion of TRPA1 mRNA was confirmed using reverse transcription quantitative real-time PCR (RT-qPCR).

To evaluate the involvement of macrophages, transgenic Macrophage Fas-Induced Apoptosis (MaFIA) mice (C57BL/6-Tg(Csf1r-EGFP-NGFR/FKBP1A/TNFRSF6)2Bck/J, stock No: 005070, RRID: IMSR_JAX:005070, Jackson Laboratories) were used. These transgenic mice express a mutant human FK506 binding protein 1A, 12kDa (FKBP12)-Fas inducible suicide/apoptotic system, driven by the mouse Csf1r promoter conjugated with a green fluorescent protein (GFP), which preferentially binds the B/B dimerizing agent (B/B-HmD, AP20187) (Diatech Labline s.r.l.). Treatment of mice with AP20187 induces the dimerization of the suicide protein to activate the cytoplasmic FKBP12-Fas fragments, leading to the apoptosis of transgene-expressing cells and consequent macrophage depletion (Burnett et al., 2004).

The group size of n = 6 mice for behavioral experiments was determined by sample size estimation using G Power [v3.1; (Faul et al., 2007)] to detect the size effect in a *post-hoc* test with type 1 and 2 error rates of 5 % and 20 %, respectively. Allocation concealment of mice into the vehicle(s) or treatment groups was performed using a randomization procedure (http://www.randomizer.org/). The assessors were blinded to the identity of the animals (genetic background or allocation to treatment groups). None of the animals were excluded from the study. Behavioral studies followed Animal Research: Reporting of *In Vivo* Experiments (ARRIVE) guidelines (McGrath and Lilley, 2015). Animal experiments and sample collections were carried out according to the European Union (EU) guidelines for animal care procedures and Italian legislation (DLgs 26/2014) application of the EU Directive 2010/63/EU.

All animal studies were approved by the Animal Ethics Committee of the University of Florence and the Italian Ministry of Health (permit no. 1146/2020-PR). The use of FFPE sections of human cutaneous tissues was approved by the Local Ethics Committee of the Florence University Hospital (Area Vasta Toscana Centro) (18271_bio/2020), according to the Helsinki Declaration, and informed consent was obtained.

2.2. Cell Lines

Human Schwann cells (HSCs) (#P10351; Innoprot, Derio, Spain) were grown and maintained in Schwann cell medium (#P60123, Innoprot) at 37 °C with 5 % CO_2 and 95 % O_2. Cells were passaged at 90 % confluence and discarded after 12 passages (De Logu et al., 2017).

Naïve E0771 (CRL-6475; RRID: CVCL_0159, American Type Culture Collection [ATCC]) murine breast carcinoma cells were cultured in Dulbecco's modified Eagle medium (DMEM) containing fetal bovine serum (FBS, 10 %) and penicillin–streptomycin (10,000 U/100 mg/mL) at 37 °C with 5 % CO_2 in a humidified atmosphere.

GFP-expressing E0771 cells were generated by lentiviral transduction. Briefly, human embryonic kidney 293 cells (HEK293T; #CRL3216™; ATCC, Manassas, VA, USA) were grown in DMEM containing FBS (10 %) and L-glutamine (2 mM) and transfected when a confluence of approximately 6×10^5 cells was reached in a 100 mm petri dish. The transfection mix contained reduced serum medium (1 mL) (#11058021 Opti-MEM™; Thermo Fisher Scientific, Waltham, MA, USA), 9.5 μg/mL packaging plasmid (#12260 psPAX2; Addgene, Watertown, MA, USA), 5 μg/mL envelope plasmid (#35616, pCAG-VSVG; Addgene), 15 μg/mL EF1a-gfp-2a-puro (#129443; Addgene), and 45 μg/mL polyethylenimine (PEI) (#23966; Polysciences, Warrington, PA, USA). After overnight incubation, 10 mL of fresh medium was added to the cell culture. The transfected cells were maintained at 37 °C in 5 % CO_2 and 95 % O_2 for a further 48 h. Then, the supernatant was collected and filtered using a 0.45 μm polyethersulfone filter (PES) and used to infect E0771 cells previously plated (50 % of confluency) on a 100-mm petri dish for 24 h. Finally, the medium containing the

lentivirus was discarded and a fresh medium with puromycin (1 μg/mL) was added to the cell culture to select E0771 GFP$^+$ cells.

Human breast cancer cells, MDA-MB-231 (#HTB-26™; ATCC), and the murine macrophage cell lineage, RAW 264.7 (#TIB-71™; ATCC), were grown in DMEM supplemented with FBS (10 %), L-glutamine (2 mM), penicillin (100 U/mL), and streptomycin (100 mg/mL) at 37 °C in 5 % CO_2 and 95 % O_2. To induce osteoclast differentiation, RAW 264.7 cells were cultured at a density of 2 × 10^5 cells/mL and treated with lipopolysaccharide (LPS; Lipopolysaccharide from *Escherichia coli* O55: B5 L6529) (100 ng/mL) for 3 d (Islam et al., 2007). The human monocytic U937 cell line (#CRL-1593.2™; ATCC) was maintained at 37 °C, 5 % CO_2, and 95 % O_2 in RPMI-1640 medium supplemented with heat-inactivated FBS (10 %), L-glutamine (2 mM), 4-(2-hydroxyethyl)-1-piperazineethanesulfonic acid (HEPES; 10 mM), and sodium pyruvate (1 mM). Osteoclast differentiation of U937 cells was induced by stimulation with phorbol 12-myristate 13-acetate (48 nM) for 2 d and then with 1,25-dihydroxyvitamin D3-13C3 (10 nM) for another 3 d (Amoui et al., 2004). All cells were used when received without further authentication. Non-metastatic mouse melanoma cells, B16-F0, were kindly donated by Prof C. Sansone (Institute of Biomolecular Chemistry, CNR, Naples, Italy) and were grown in DMEM supplemented with FBS (10 %) and L-glutamine (2 mM) before injection.

2.3. Cancer cell inoculation

For inoculation, 20 μL of E0771 breast carcinoma cells (2 × 10^5 cells) or B16-F0 melanoma cells (2 × 10^5 cells) were suspended in PBS and injected into the fourth right mammary fat pad of the mouse. Control groups were injected with 20 μL of PBS containing E0771 breast carcinoma cells (2 × 10^5 cells) or B16-F0 melanoma cells (2 × 10^5 cells) killed by quick freezing and thawing (twice) without cryoprotection. Both cell lines were syngeneic with the C57BL/6J mouse strain.

The tumor thickness was measured before and at day 5, 10, 15 and 20 after inoculation using a digital caliper and the tumor volume was calculated according to the formula $V = 0.52 \times \text{width}^2 \times \text{length}$, where width is the smaller of the two measurements (Nachat-Kappes et al., 2012). Body weight of inoculated or control mice was measured before and at day 5, 10, 15 and 20 after inoculation.

2.4. Treatment protocols

If not otherwise indicated, the reagents were obtained from Merck Life Science SRL (Milan, Italy). C57BL/6J (E0771 inoculated or control mice) were treated with: picropodophyllin (PPP) (20 mg/kg, i.p.) and Ro32-0432 (1 mg/kg, i.p.) or their vehicle (4 % DMSO, 4 % Tween 80 in 0.9 % NaCl) twice a day from 17 to 20 d after cell inoculation; N-tert-butyl-alpha-phenylnitrone (PBN) (100 mg/kg, i.p.), cPTIO (0.6 mg/kg i.p.), L-NAME (50 mg/kg, i.p.), Akti-1/2 (50 mg/kg, i.p.), reparixin (5 mg/kg i.p.), AP20187 (2 mg/kg i.p.), and Pexidartinib (PLX-3397) (40 mg/kg i.p.) or their vehicle (4 % DMSO, 4 % Tween 80 in 0.9 % NaCl) once a day from 10 to 20 d after cell inoculation; NT157 (50 mg/kg, i.p.) or its vehicle (4 % DMSO, 4 % Tween 80 in 0.9 % NaCl) every 2 d from 10 to 20 d after cell inoculation; neutralizing anti-IL-6 (200 μL, 1 mg/mL, i.p.) (#BE0046, clone MP5-20F3, RRID:AB_1107709 Bio X Cell, Lebanon, NH, USA), anti-TGF-β (200 μL, 1 mg/mL, i.p.) (#BE0057, clone 1D11.16.8, RRID:AB_1107757, Bio X Cell), and anti-IGF-1 monoclonal antibodies (mAb) [#05-172, clone Sm1.2, RRID: AB_309643; Millipore, Burlington, MA, USA; i.th. (5 μL) or p.n. (5 μL) (50 μg/mL)] or their vehicle (IgG1, isotype control, #BE0083, clone MOPC-21, RRID: AB_1107784; Bio X Cell) every 2 d from 10 to 20 d after cell inoculation.

In some experiments, neutralizing anti-IL-6 (200 μL, 1 mg/mL, i.p.), anti-TGF-β (200 μL, 1 mg/mL, i.p.), or their vehicles, were administered every 2 d from 2 to 10 d after cell inoculation.

Plp-CreERT$^+$ or Plp-CreERT$^-$ were treated with an intrasciatic (i.sc., 5 μL) injection of pAAV[FlexOn]-CMV-EGFP-mIGF1R[shRNA]-mCherry viral vector (2 × 10^{10} VG/mL) two weeks before E0771 cell inoculation. Adv-Cre$^+$ or Adv-Cre$^-$ mice were treated with an i.th. (5 μL) injection of pAAV[FlexOn]-CMV-EGFP-mIGF1R[shRNA]-mCherry viral vector (2 × 10^{10} VG/mL) two weeks before E0771 cell inoculation. At 20 d after E0771 cell inoculation, mice were euthanized (ketamine 200 mg/kg and xylazine 20 mg/kg, i.p.) and the sciatic nerve and DRGs were harvested for analysis. Viral infection was confirmed by immunofluorescence analysis. Only the infected cells (mCherry) were fluorescent upon examination with a red filter.

In another set of experiments, IGF-1 (0.1, 0.5, and 1 nMol) or its vehicle (0.9 % NaCl) (10 μL) was then injected (i.pl.). PPP (120 nMol), Ro32-0432 (20 nMol), PBN (670 nMol), cPTIO (200 nMol), L-NAME (1 μmol), Akti-1/2 (100 nMol), NT157 (100 nMol), and PitStop2 (500 pmol) or their vehicle (4 % DMSO, 4 % Tween 80 in 0.9 % NaCl) were administered (10 μL, i.pl.) 30 min before IGF-1 (1 nMol, i.pl.). Supplementary Table 1 provides the doses and routes of administration for all the pharmacological treatments.

2.5. Behavioral assays

2.5.1. Mechanical allodynia

The mechanical paw-withdrawal threshold was measured using von Frey filaments of increasing stiffness (0.02–2 g) applied to the plantar surface of the mouse hind paw, according to the up-and-down paradigm (Chaplan et al., 1994). The 50 % mechanical paw-withdrawal threshold (g) response was then calculated from the resulting scores.

2.5.2. Cold response

Cold sensitivity was assessed by measuring the acute nocifensive response to acetone-evoked evaporative cooling as previously described (De Logu et al., 2021). Briefly, mice were placed in a wire mesh floor cage and, after habituation, a droplet (50 μL) of acetone, formed on the flat-tip needle of a syringe, was gently touched to the plantar surface of the hind paw, and the time spent in elevation and licking of the plantar region over a 60-s period was measured. Acetone was applied three times at 10- to 15-min intervals and the average elevation/licking time was calculated.

2.5.3. Acute nociception

Immediately after i.pl. injection, mice were placed inside a plexiglass chamber, and spontaneous nociception was assessed for 10 min by measuring the time (seconds) that the animal spent licking/lifting the injected paw.

2.5.4. Open field test

The mice were acclimated to the room for 1 h before recording. Mice were introduced into individual activity transparent acrylic chambers (30.48 × 30.48 × 30.48 cm) aligned horizontally or vertically, with each chamber housing a single mouse for analysis. The mice were placed in the chamber and their activity was recorded for 10 min with a digital camera. Videotapes were analyzed using an open-source video tracking system (Zhang et al., 2020). Spontaneous locomotor activity, measured as the cumulative distance traveled, and time spent in the inner zone in the open field apparatus was analyzed. The inner zone is defined as a square comprising the inner 50 % of the area.

2.5.5. Rota-rod test

For the locomotor function assessment animals were trained on a rotarod apparatus (Ugo Basile) 24 h before the test. The day of the experiment, each mouse was individually placed on the apparatus, which accelerated from 4 to 40 rpm over the trial time of 300 s. Latency to fall was evaluated and recorded for three trials.

2.6. Virus Generation

The AAV plasmid for stable RNAi of mouse IGF1R was obtained by

choosing Cre-lox conditional shRNA expression based on the FLEX switch system (Schnütgen et al., 2003). The construct pAAV[FlexOn]-CMV-EGFP-mIGF1R[shRNA]-mCherry (#VB210916-1096bqm) was obtained using VectorBuilder (mIGF1R shRNA; 5′ AAGCTGTGTGTCTCCGAAATTTTA-CATCTGTGGCTTCACTAAAATTTCGGAGACACACAGCTG-3′). The detailed method is described in the Supplementary Information.

2.7. Primary culture of mouse Schwann cells (MSCs)

MSCs were isolated from the sciatic nerve of C57BL/6J mice, as previously described (De Logu et al., 2017). Briefly, the sciatic nerve was dissected, the epineurium was removed, and nerve explants were divided into 1 mm segments and dissociated enzymatically using collagenase (0.05 %) and hyaluronidase (0.1 %) in Hank's balanced salt solution (HBSS) (2 h, 37 °C). Cells were collected by centrifugation (150*g*, 10 min, 20–25 °C), and the pellet was resuspended and cultured in DMEM containing fetal calf serum (10 %), L-glutamine (2 mM), penicillin (100 U/mL), streptomycin (100 mg/mL), neuregulin (10 nM), and forskolin (2 μM). Three days later, cytosine arabinoside (Ara-C, 10 mM) was added to remove the fibroblasts. Cells were cultured at 37 °C in 5 % CO_2 and 95 % O_2. The culture medium was replaced every 3 d, and the cells were used after 15 d of culture.

2.8. Primary culture of mouse dorsal root ganglion (DRG) neurons

Mouse DRGs (combined cervical, thoracic, and lumbar) were bilaterally excised under a dissection microscope and enzymatically digested using 2 mg/mL of collagenase type 1A and 1 mg/mL of papain in HBSS for 35 min at 37 °C. Ganglia were disrupted by several passages using a series of syringe needles (23–25G). Mouse DRG neurons were then pelleted by centrifugation at 180*g* for 5 min at room temperature and resuspended in DMEM supplemented with Ham's F12 containing 10 % heat-inactivated FBS, 100 U/mL of penicillin, 0.1 mg/mL streptomycin, and 2 mM L-glutamine added with 100 ng/mL nerve growth factor, and 2.5 mM cytosine-b-D-arabino-furanoside free base (ARA-C), and maintained at 37 °C in 5 % CO_2 and 95 % O_2 for 3 d before being used for Ca^{2+} imaging experiments.

2.9. Triple co-culture

Triple co-culture experiments were performed using $OMEGA^{ACE}$ devices (#eN-oace-002; eNUVIO Inc., Montréal, Canada). The detailed method is described in the Supplementary Information.

2.10. Ca^{2+} imaging

The detailed method is described in the Supplementary Information.

2.11. Nitric oxide in vitro imaging

A fluorescence probe for NO imaging (FP-NO) in live cells was synthesized as reported previously (Han et al., 2019; Long et al., 2015) (The detailed method is described in the Supplementary Materials and Methods section). In a set of experiments, human Schwann cells (HSCs) and mouse DRG neurons were plated on poly-L-lysine-coated (8.3 μM) 35-mm glass coverslips and maintained at 37 °C in 5 % CO_2 and 95 % O_2 for 24 h. Cells were loaded for 30 min with FP-NO (5 μM) and added to Hank's balanced salt solution (HBSS) at pH 7.4. Cells were washed and transferred to a chamber on the stage of a fluorescent microscope for recording (Axio Observer 7; with a fast filterwheel and Digi-4 lens to record excitations; ZEISS, Stuttgart, Germany) and were exposed to human or mouse IGF-1 (100 nM) or its vehicle (0.9 % NaCl) for 0.5 h. HSCs were exposed to human IGF-1 also in the presence of PPP (10 nM) or its vehicle (0.0005 % DMSO). The ΔF/F0 ratio was calculated for each experiment and the results were expressed as the area under the curve (AUC).

In another set of experiments, HSCs were plated in 96-well black wall clear bottom plates (5×10^5 cells/well; Corning Life Sciences, Tewksbury, MA, USA) and maintained in 5 % CO_2 and 95 % O_2 (24 h, 37 °C). The cells were incubated for 30 min with FP-NO (5 μM). The culture medium was replaced with HBSS supplemented with NT157 (3 μM), Akti-1/2 (100 nM), and L-NAME (10 μM) or their vehicle (0.1 % DMSO) for 20 min at 20–25 °C, and then stimulated with human IGF-1 (100 nM) or its vehicle (0.9 % NaCl) for 0.5 h. Diethylamine NONOate (2-[N,N-diethylamino]-diazenolate 2-oxide sodium salt hydrate) (10 μM) was used as a positive control. The measurements were performed using a fluorescence plate reader (FlexStation 3 Multi-Mode Microplate Reader; Molecular Devices, San Jose, CA, USA) with SoftMax® Pro 7 software (Molecular Devices) with the following settings: λ excitation, 436 nM and λ emission, 475 nM. The results are expressed as arbitrary units (A. U.).

2.12. H_2O_2 in vitro imaging

A genetically encoded probe for H_2O_2-HyPer [HyPer7.2 (Pak et al., 2020), kindly donated by Dr. Emrah Eroglu, Harvard Medical School, Boston, US] was used on live cells. HSCs and mouse DRG neurons were plated on poly-L-lysine-coated (8.3 μM) 35-mm glass coverslips and transfected with DNA (2 μg) of HyPer7.2 using jetOPTIMUS® DNA transfection reagent (#55-250; Polyplus, Lexington, MA, USA). After 24–48 h, the HSCs were washed and transferred to a chamber on the stage of a fluorescent microscope for recording (Axio Observer 7; with a fast filterwheel and Digi-4 lens to record excitations; ZEISS, Stuttgart, Germany). Cells were exposed to human or mouse IGF-1 (1 μm), or its vehicle (0.9 % NaCl), and H_2O_2 variations were monitored for approximately 1 h. HSCs experiments were performed also in the presence of PPP (10 nM), Akti-1/2 (100 nM), or A967079 (50 μM). Results were expressed as the percentage increase in the $ratio_{408/455}$ over the baseline normalized to the maximum effect, induced by H_2O_2 (10 μM) added at the end of each experiment.

2.13. Protein extraction and western immunoblot assay

HSCs were plated on 60 mm culture dishes and maintained at 37 °C in 5 % CO_2 and 95 % O_2 until 90 % confluence. The cells were serum-starved for 4 h in Schwann cell medium without FBS and then treated with IGF-1 (100 nM) for 10 min. The detailed method is described in the Supplementary Information.

2.14. Immunofluorescence

The detailed method is described in the Supplementary Information.

2.15. RNAscope

RNAscope assays were performed according to the manufacturer's protocol. The detailed method is described in the Supplementary Information.

2.16. Plasma Ca^{2+} level

The total plasma Ca^{2+} content was measured at 20 d after cells inoculation using a colorimetric Ca^{2+}assay kit (#ab102505; Abcam, Cambridge, UK), according to the manufacturer's protocol.

2.17. IGF-1, IL-6, TGF-β-M-CSF assays

The IGF-1 contents were assayed in the bone and sciatic nerve tissue homogenates at 20 d after cancer cell inoculation and in the cultured medium using a single-analyte enzyme-linked immunosorbent assay kit (#ab100695 and #ab100545, Abcam, Cambridge, UK) according to the

manufacturer's protocol. Data are expressed as pg/mg of protein and pg/mL. IL-6 and TGF-β levels were assayed in the bone and sciatic nerve tissue homogenates at 20 d after cancer cell inoculation using a single-analyte enzyme-linked immunosorbent assay kit (#ab100713 and #ab119557, respectively, Abcam) according to the manufacturer's protocol. The samples were assayed in triplicate. Data are expressed as pg/mg of protein. M-CSF content was assayed in the sciatic nerve tissue homogenates at 20 d after cancer cell inoculation and in the cultured medium using a single-analyte enzyme-linked immunosorbent assay kit (#ab199084 ad #ab245714 Abcam) according to the manufacturer's protocol. Data are expressed as pg/mg of protein and pg/mL.

2.18. H_2O_2 assay

H_2O_2 levels were assessed in sciatic nerve tissue homogenates and cultured medium using the Amplex Red® assay (Invitrogen, Waltham, MA, USA), according to the manufacturer's protocol. Fluorescence excitation and emission were measured at 540 and 590 nM, respectively. H_2O_2 production was calculated using the H_2O_2 standard and expressed as nMol/mg protein or µmol/L.

2.19. Nitric oxide assay

The NO content was determined in sciatic nerve tissue homogenates at 20 d after cancer cell inoculation and in the cultured medium using a colorimetric assay kit (#ab272517; Abcam, Cambridge, UK) according to the manufacturer's protocol. Data are expressed as µmol/L/mg of protein or µmol/L.

2.20. RT-qPCR

Total RNA was extracted from HSCs, primary MSCs, mice sciatic nerves, and DRGs using the RNeasy Mini Kit (Qiagen SpA, Hilden, Germany), according to the manufacturer's protocol. The detailed method is described in the Supplementary Information.

2.21. Statistical analysis

The results are expressed as the mean ± SEM. For multiple comparisons, a one-way ANOVA followed by a post-hoc Bonferroni's test or Dunnett's test was used. The two groups were compared using Student's *t*-test. For behavioral experiments with repeated measures, a two-way mixed-model ANOVA followed by a post-hoc Bonferroni's test was used. Statistical analyses were performed on raw data using GraphPad Prism 8 (GraphPad Software Inc., San Diego, CA, USA). *P*-values less than 0.05 ($P < 0.05$) were considered significant. The statistical tests used and sample size for each analysis are shown in the Fig. legends.

3. Results

3.1. IGF-1 in MBCP

Inoculation of E0771 breast carcinoma cells into the mammary gland (intramammary) of C57BL/6J female mice (C57) (Fig. 1a) induced a time-dependent increase in mammary tumor mass, mainly due to tumor growth (Fig. 1b). Tumor evolution was associated with a progressive increase in hind paw mechanical/cold hypersensitivity and a reduction in spontaneous locomotor activity (cumulative distance traveled) and thigmotaxis behavior (time spent in the inner zone), two indices of non-stimulus-evoked pain-like behavior (Antoniazzi et al., 2019; Deuis et al., 2017; Huang et al., 2013; Zhang et al., 2020) (Fig. 1c–f). Hereafter, these behaviors are collectively defined as pain-like behaviors. No impairment in motor coordination was observed in E0771 cell-inoculated mice (E0771-mice) compared to control mice (Supplementary Fig. 1a). Control mice, inoculated with E0771-killed cells, showed no increase in mammary thickness, nor in measurable pain-like behaviors (Fig. 1b–f). As pain-like behaviors plateaued between 16–20 d after E0771 cell inoculation, if not otherwise specified, all outcome measures reported hereafter were assessed 20 d after inoculation. Unless otherwise specified, all experiments were conducted in C57 mice. Body weight of E0771- or control mice at the beginning and end of the protocol was similar (Supplementary Fig. 1b)

Mice inoculated with E0771-green fluorescent protein (GFP) cells showed a time-dependent increase in the fluorescent metastatic mass in the femoral head (Fig. 1g). The presence of bone metastasis in E0771-mice was further supported by increased plasma Ca^{2+} levels (Fig. 1h). To verify that the source of pain-like behaviors was the metastasis and not the primary tumor, poor-metastatic melanoma cells (B16-F0) (Nicolson et al., 1978) were inoculated in the C57 fat pad. Twenty days after cell inoculation, primary tumor masses of E0771 and B16-F0 mice were comparable (Fig. 1b and Supplementary Fig. 1c). However, B16-F0-mice did not show any pain-like behaviors or increased plasma Ca^{2+} levels (Supplementary Fig. 1d-h). This data confirms that the primary tumor in the fat pad is not *per se* sufficient to induce pain-like behaviors in C57 mice. In E0771-mice, the development of pain-like behaviors was associated with increased levels of osteolysis biomarkers, including IGF-1, IL-6, and TGF- β, in both bone and sciatic nerve tissue homogenates (Fig. 1i and Supplementary Fig. 1i and j). We then explored which of these mediators were implicated in pain-like behaviors. Repeated administration of the IGF-1 receptor (IGF-1R) inhibitor, picropodophyllin (PPP), attenuated E0771 cell-evoked pain-like behaviors (Fig. 1j-m), without affecting the growth of the primary tumor size (Fig 1n) or femur metastasis (Fig. 1o). Furthermore, repeated administration of IL-6 or TGF- β neutralizing antibodies (from days 10 to 20) had no effect on pain-like behaviors or primary tumor growth (Supplementary Fig. 1k-t). To test the effect of IL-6 or TGF-β in the initial development of pain-like behaviors, we administered the neutralizing antibodies from day 2 to day 10 in E0771- mice. No significant difference was observed in paw mechanical/thermal hypersensitivity after these treatments compared to control (Supplementary Fig. 1u-x). The results suggest that pain-like behaviors depend solely on increased IGF-1 levels and are unrelated to the expansion of femur metastases.

3.2. IGF-1-induced hypersensitivity is mediated by Schwann cell IGF-1R

IGF-1 has been reported to contribute in various rodent pain models (Forster et al., 2019; Kohno et al., 2022; Sugawara et al., 2019; Takayama et al., 2011; Zhang et al., 2014), including bone pain induced by the inoculation of mammary carcinoma cells into the tibial cavity (Li et al., 2014). The proalgesic action of IGF-1 has been proposed to have a direct action on nociceptors (Zhang et al., 2014). However, the pathways by which IGF-1 signals pain remain unknown. Owing to the emerging critical role of Schwann cells in sustaining mechanical hypersensitivity in different chronic pain models in mice (De Logu et al., 2019; De Logu et al., 2021; De Logu et al., 2022; De Logu et al., 2017), and the presence of IGF-1R in Schwann cells (Syroid et al., 1999), we hypothesized that Schwann cells encode the IGF-1 signal that elicits pain-like behaviors in the present MBCP mouse model.

First, we showed the proalgesic activity of IGF-1 in the peripheral and not in the central nervous system in E0771-mice. Repeated perineural (p.n.), but not intrathecal (i.th.), administration of an IGF-1-neutralizing antibody reduced pain-like behaviors in E0771-mice (Supplementary Fig. 2a–d and f–i), while tumor growth was unaffected by both treatments (Supplementary Fig. 2e and j). These findings indicate the peripheral nervous system as the primary site of IGF-1 proalgesic action. Second, to identify the cell(s) responsible for cancer-evoked and IGF-1-mediated pain-like behaviors, we confirmed the expression of IGF-1R mRNA and protein in human and mouse cultured Schwann cells and in *ex-vivo* nerve trunks and mouse DRGs (Fig. 2a–e). Then, by using AAV-based Cre-dependent shRNA, we selectively silenced IGF-1R in mice expressing Cre recombinase, either in Schwann cells (Plp-Cre) or primary sensory neurons (Adv-Cre), thus generating

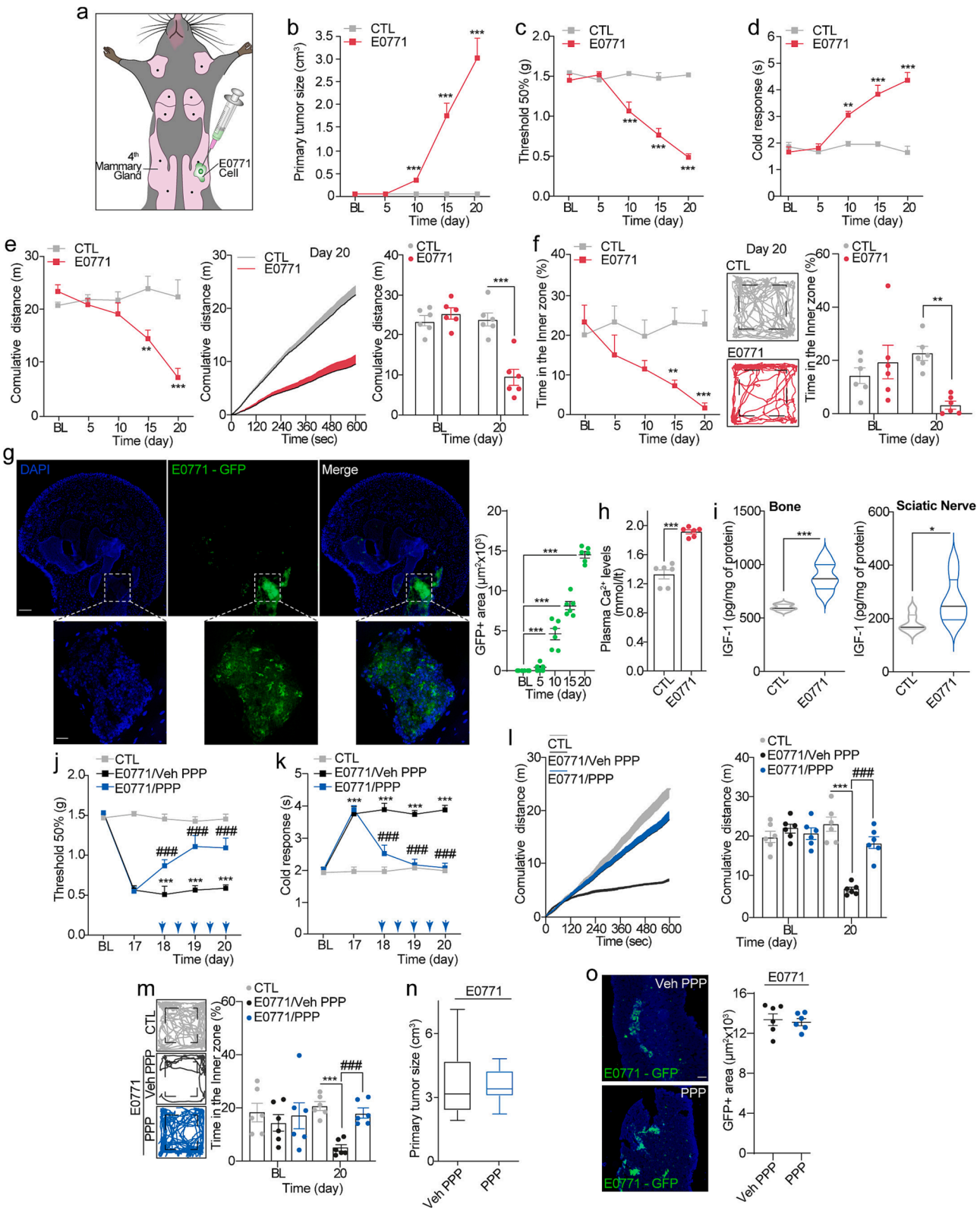

Fig. 1. E0771 cells intramammary inoculation induces bone metastatic cancer pain mediated by IGF-1 (a) Graphical illustration of intramammary E0771 cell inoculation. (b) Time-dependent increase in primary tumor size and (c) mechanical and (d) cold allodynia after E0771 cell intramammary inoculation or control (CTL) in C57BL/6J mice. (e) Cumulative distance and (f) time spent in the inner zone after E0771 cell inoculation or CTL in C57BL/6J mice (n = 6 mice per group). (g) Whole slide images of E0771-GFP^{+} cells in the femur head 20 d after E0771 cell inoculation in C57BL/6J mice (Scale bar: 50 µm, inset 20 µm) and time-dependent increase of the bone metastasis tumor mass (GFP^{+}area µm^2 × 10^3). (h) Plasma Ca^{2+} levels and (i) bone and sciatic nerve tissue homogenate IGF-1 content 20 d after E0771 cell inoculation or CTL in C57BL/6J mice. (j) Mechanical and (k) cold allodynia, (l) cumulative distance, (m) time spent in the inner zone, (n) primary tumor size and (o) representative images and bone metastasis tumor mass (GFP^{+}area µm^2 × 10^3) after E0771 cell inoculation or CTL in C57BL/6J mice treated with PPP/vehicle (i.p.). (Scale bar: 50 µm) (n = 6 mice per group). Mean ± SEM. $^{*}P < 0.05$, $^{**}P < 0.01$, $^{***}P < 0.001$ vs. CTL, BL; $^{\#\#\#}P < 0.001$ vs. E0771, E077/vehicle PPP.

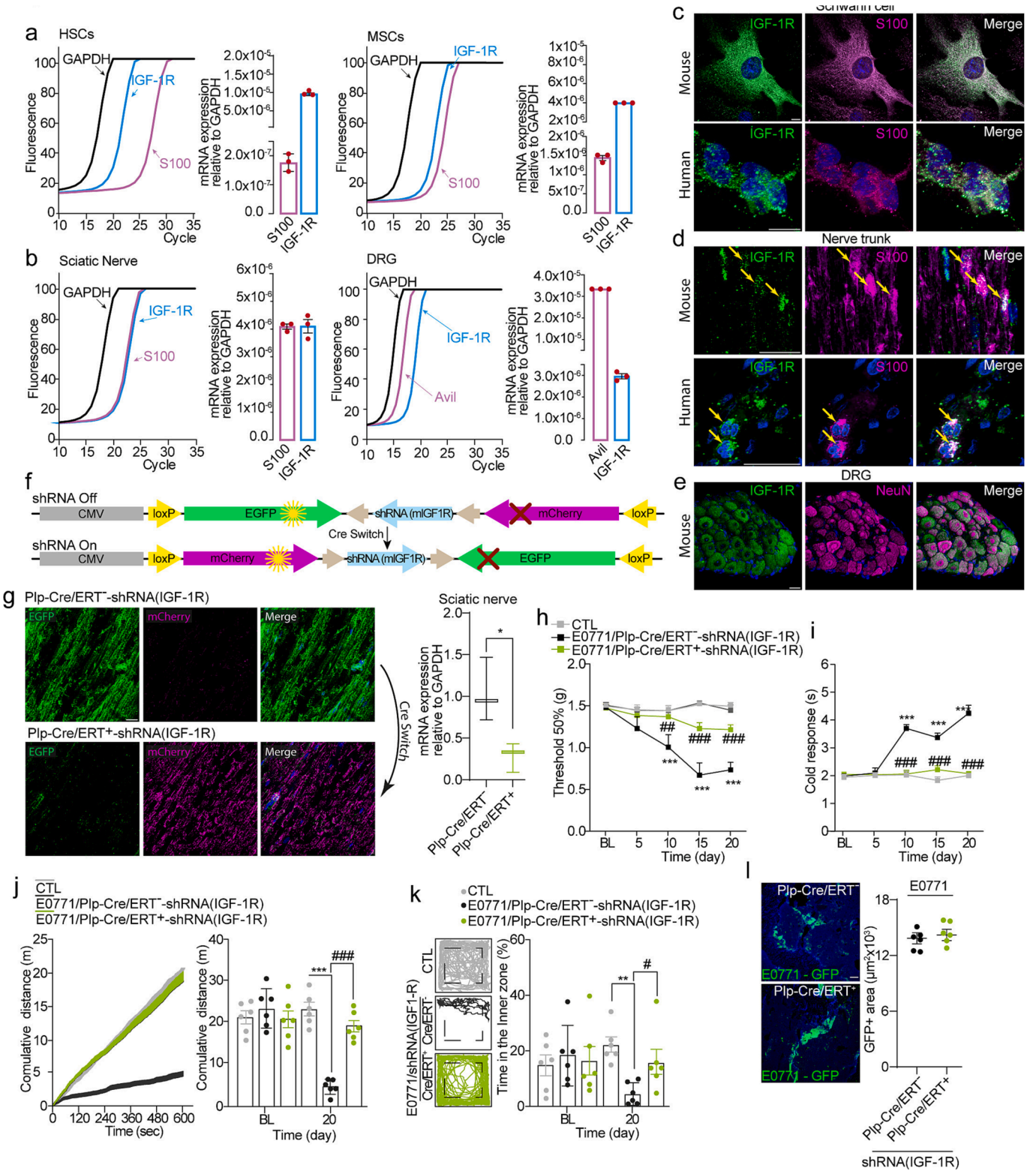

Fig. 2. Schwann cell IGF-1R modulates E0771 bone metastatic cancer pain (a) IGF-1R mRNA relative expression in primary HSCs and MSCs and (b) mouse sciatic nerve and dorsal root ganglia (DRG) tissue homogenates (n = 3 replicates). (c) Immunocytochemistry of IGF-1R in primary HSCs and MSCs (Scale bar: 10 μm) (n = 3 replicates). Images of IGF-1R expression in (d) human intraepidermal nerve and mouse sciatic nerve and (e) mouse DRGs (Scale bar: 20 μm) (n = 3 subjects). (f) Diagram of AAV-(loxP-shRNA)IGF-1R vector pre- and post-Cre switch. (g) Representative images of Cre switch and IGF-1R mRNA relative expression in mouse sciatic nerve of Plp-Cre/ERT^{-} and Plp-Cre/ERT^{+} mice infected with AAV-(loxP-shRNA)IGF-1R viral vector (Scale bar: 20 μm). (h) Mechanical and (i) cold allodynia, (j) cumulative distance (k) time spent in the inner zone and (l) representative images and bone metastasis tumor mass (GFP^{+}area μm^2 × 10^3) after E0771 cell inoculation or control (CTL) in Plp-Cre/ERT^{-} and Plp-Cre/ERT^{+} infected with AAV-(loxP-shRNA)IGF-1R [E0771/Plp-Cre/ERT^{-}-shRNA(IGF-1R) and E0771/Plp-Cre/ERT^{+}-shRNA (IGF-1R)] (Scale bar: 50 μm) (n = 6 mice per group). Mean ± SEM. $^{*}P < 0.05$, $^{**}P < 0.01$, $^{***}P < 0.001$ vs. CTL; $^{\#}P < 0.05$, $^{\#\#\#}P < 0.001$ vs. E0771/Plp-Cre/ERT^{-}-shRNA(IGF-1R).

Plp-Cre/ERT^{+}-shRNA(IGF-1R) and Adv-Cre-shRNA(IGF-1R) mice, respectively (Fig. 2f and g and Supplementary Fig. 2k). IGF-1R silencing was confirmed by RT-qPCR (Fig. 2g and Supplementary Fig. 2k). Intrasciatic (i.sc.) administration of AAV-shRNA(IGF-1R) in Plp-Cre mice, but not i.th. administration of AAV-shRNA(IGF-1R) in Adv-Cre mice, attenuated pain-like behaviors in E0771-mice (Fig. 2h–k and Supplementary Fig. 2l–o). The growth of bone metastasis was unaffected by selective silencing of Schwann cell IGF-1R (Fig. 2l). These findings pointed to IGF-1R in Schwann cells, but not in nociceptors, as the mediator of pain-like behaviors.

To identify the sequential events underlying pain-like behaviors, we set up a triple co-culture chamber containing mouse or human: breast cancer cells (E0771 or MDA-MB-231, respectively), osteoclasts (RAW 264.7 or U937, respectively), and Schwann cells. This setup allowed unidirectional flux from breast cancer cells to osteoclasts, and finally to Schwann cells (Fig. 3a and f). The absence of cancer cells or osteoclasts, but not Schwann cells, attenuated IGF-1 release (Fig. 3b and g). Previous evidence indicates that IL-8, IL-11, and TNF- β (Le Pape et al., 2016; Weilbaecher et al., 2011) are released from cancer cells and might be responsible for IGF-1 release. In the triple chamber, IL-8, but not IL-11 or TNF-α, inhibition attenuated the increase in IGF-1 in the medium (Supplementary Fig. 2p). *In vivo* findings strengthened the role of IL-8 as an antagonist of the IL-8 receptor (CXCR1/2), reparixin, reduced pain-like behaviors, and left unaffected primary tumor growth in E0771-mice (Supplementary Fig. 2q–u), thus indicating that cancer cell-derived IL-8 releases IGF-1 from osteoclasts.

Recently, we reported the essential role of oxidative stress generated by Schwann cells in hypersensitivity in various mouse pain models (De Logu et al., 2021; De Logu et al., 2017). Using the triple chamber, we found that the removal of each cell type reduced the H_2O_2 increase (Fig. 3c and h), leading us to conclude that Schwann cells, the last cell bathed by the fluid, generated an oxidative stress burst. The finding that treatment with the IGF-1R antagonist, PPP, prevented the release of H_2O_2, but not IGF-1 (Fig. 3d and e and i and j), suggests that osteoclast-derived IGF-1 increases oxidative stress by targeting Schwann cell IGF-1R. Our *in vivo* experiments corroborated these findings. Intraperitoneal (i.p.) administration of the antioxidant phenyl-alpha-tert-butyl nitrone (PBN) abated pain-like behaviors in E0771-mice (Fig. 3k–n) by reducing H_2O_2 sciatic nerve content (Fig. 3o), without affecting IGF-1 increase in either bone or sciatic nerve tissue homogenates (Fig. 3p) and primary tumor growth (Fig. 3q).

3.3. Dichotomous proalgesic pathways of IGF-1R in DRG neurons (spontaneous nociception) and Schwann cells (mechanical/cold hypersensitivity)

To better delineate the IGF-1/Schwann cell pathway, both *in vivo* and *in vitro* experiments were performed. As previously reported (Kavran et al., 2014), we observed that IGF-1 stimulation of human Schwann cells induced IGF-1R trans-phosphorylation and the activation of insulin receptor substrate 1 (IRS-1) and serine/threonine kinase (Akt) (Fig. 4a and b). We also found that IGF-1R activation in human Schwann cells caused endothelial nitric oxide synthase (eNOS) phosphorylation and the release of NO and H_2O_2 (Fig. 4c–k). Both NO and H_2O_2 release elicited by IGF-1 from human Schwann cells was attenuated in the presence of the IGF-1R antagonist, PPP, the IRS-1 inhibitor, NT157, the Akt inhibitor, Akti-1/2, and the eNOS inhibitor, L-NAME (Fig. 4d–k). It has been proposed that IGF-1R elicits nociception by activating protein kinase Cα (PKCα)in DRG neurons *via* phosphorylation of the voltage-gated T-type Ca^{2+}(CaV3) channels (Zhang et al., 2014). In our experiments, the PKC inhibitor, Ro32-0432, did not affect H_2O_2 generation induced by IGF-1 (Fig. 4l), indicating that a PKC-independent pathway mediates IGF-1 responses in Schwann cells. Conversely, we confirmed that IGF-1 induces a Ca^{2+}response in DRG neurons, which was abolished by PKC inhibition (Fig. 4m). IGF-1 stimulation was unable to induce a significant increase in NO and H_2O_2 in cultured DRG neurons (Supplementary Fig. 3a and b).

Next, we explored the Schwann cell/IGF-1R pathway in mice. IGF-1 injection (i.pl.) dose-dependently produced an early and transient (10 min) spontaneous nociception, followed by a prolonged (~4 h) mechanical/cold hypersensitivity, which were attenuated by pretreatment with the IGF-1R inhibitor, PPP (Fig. 5a–f). IGF-1 (i.pl.) also increased NO and H_2O_2 levels in sciatic nerve homogenates, all effects reduced by PPP (Fig. 5g and h). A key result was obtained after IGF-1 (i.pl.) injection in mice with selective silencing of IGF-1R in Schwann cells (Plp-Cre/ERT^{+}-shRNA(IGF-1R)). Sustained mechanical/cold hypersensitivity, but not acute spontaneous nociception, evoked by IGF-1 was attenuated in these mice (Fig. 5i–k). Conversely, in mice with selective silencing of IGF-1R in primary sensory neurons (Adv-Cre-shRNA(IGF-1R)), acute spontaneous nociception evoked by IGF-1 was attenuated, whereas mechanical/cold allodynia remained unaffected (Supplementary Fig. 4a–c). In addition, pretreatment with Ro32-0432 attenuated spontaneous nociception without affecting mechanical/cold hypersensitivity (Supplementary Fig. 4d–f).

Pretreatment with the IRS-1 inhibitor, NT157, reduced both spontaneous nociception and mechanical/cold hypersensitivity, whereas Akti-1/2, L-NAME, and cPTIO only reduced mechanical/cold hypersensitivity, but not spontaneous nociception, evoked by IGF-1 (i.pl.) in mice (Fig. 5l–w). IRS-1 is known to inhibit IGF-1R internalization in endosomes by suppressing IGF-1R recruitment in clathrin structure, thus prolonging the permanence of activated IGF-1R to the cell surface (Dam et al., 2020; Yoneyama et al., 2018), a phenomenon likely associated with mechanical/cold hypersensitivity. In agreement with these findings, pretreatment with the clathrin-dependent endocytosis inhibitor, Pitstop2, did not affect spontaneous IGF-1-evoked nociception nor mechanical/cold hypersensitivity (Supplementary Fig. 5a–c). NT157, which, by inhibiting IRS-1, promotes IGF-1R internalization, reduced both spontaneous nociception and mechanical/cold hypersensitivity. However, Pitstop2 restored only spontaneous nociception and failed to restore mechanical/cold hypersensitivity (Supplementary Fig. 5d–f). This data supports the role of IGF-1R clathrin-dependent endocytosis, and the canonical PKC-dependent pathway encoded by neuronal IGF-1R solely in spontaneous nociception. In the triple chamber, NT157, Akti-1/2, L-NAME, and cPTIO attenuated the increase in NO and H_2O_2, while the increase in IGF-1 was not affected (Fig. 6a–g). NT157, Akti-1/2, L-NAME, and cPTIO reduced NO and H_2O_2 levels *in vivo* in sciatic nerve homogenates (Supplementary Fig. 5g and h) and attenuated all pain-like responses observed in E0771-mice (Supplementary Fig. 5i–x). Altogether, present data highlight a novel pathway resulting from IGF-1R activation in Schwann cells, which promotes mechanical/cold hypersensitivity by Akt and eNOS phosphorylation and NO and ROS release.

3.4. NO release by IGF-1 in Schwann cells activates TRPA1 to generate oxidative stress

The final step of the IGF-1R/Schwann cell pathway involves the release of H_2O_2. Recently, we showed that eNOS activation in Schwann cells, elicited by calcitonin gene-related peptide (CGRP), releases NO. NO directly, or *via* reactive nitrogen species (Eberhardt et al., 2014), stimulates Schwann cell TRPA1, which amplifies the oxidative stress signal to sustain periorbital mechanical allodynia (De Logu et al., 2022). RNAscope analysis provided further evidence of TRPA1 mRNA expression in Schwann cells of mouse sciatic nerve and DRG neurons (Fig. 7a). Stimulation of human Schwann cells with breast cancer cell/osteoclast-conditioned medium elicited a delayed TRPA1-mediated Ca^{2+} response that was inhibited by PPP, NT157, Akti-1/2, L-NAME, cPTIO, and in a Ca^{2+}-free medium, thus recapitulating results obtained by IGF-1R activation (Fig. 7b–f). Stimulation of human Schwann cells with IGF-1 produced an increase in H_2O_2, which was prevented by the TRPA1 selective antagonist, A967079 (Fig. 7g). In the triple chamber, A967079 attenuated the release of H_2O_2, but not that of IGF-1 or NO (Fig. 7h), suggesting that TRPA1 activation and oxidative stress generation are

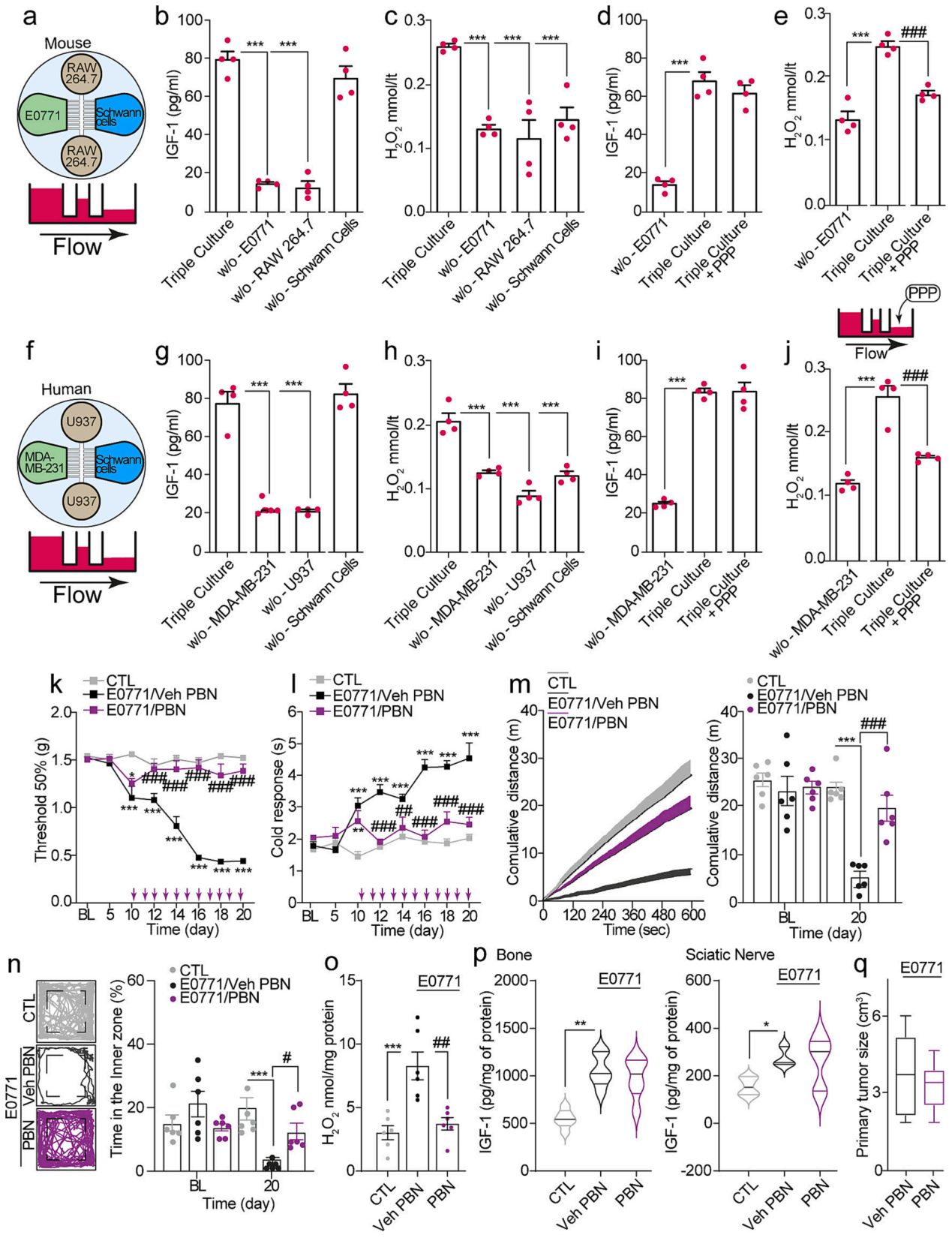

Fig. 3. IGF-1 from osteoclast induces Schwann cell H_2O_2 release (a) Diagram of the triple co-culture chamber with mouse (E0771, RAW264.7, and Schwann cells) and (f) human (MDA-MB-231, U937, and Schwann cells) cells. IGF-1 levels in (b) mouse and (g) human triple co-culture without each of the three cell cultures. H_2O_2 levels in (c) mouse and (h) human triple co-culture without each of the three cell cultures. IGF-1 and H_2O_2 levels in (d, e) mouse and (i, j) human triple co-culture after Schwann cell treatment with PPP (n = 4 replicates). (k) Mechanical/(l) cold allodynia, (m) cumulative distance, (n) time spent in the inner zone after E0771 cell inoculation or control (CTL) in C57BL/6J mice treated with PBN/vehicle (i.p.). (o) H_2O_2 levels in the sciatic nerve, (p) IGF-1 levels in bone and sciatic nerve tissue homogenates and (q) primary tumor size in C57BL/6J mice at 20 d after E0771 cell inoculation or CTL treated with PBN/vehicle (i.p.) (n = 6 mice per group). Mean ± SEM. $^{*}P < 0.05$, $^{**}P < 0.01$, $^{***}P < 0.001$ vs. CTL, Triple Culture; $^{\#}P < 0.05$, $^{\#\#}P < 0.01$, $^{\#\#\#}P < 0.001$ vs. E0771/vehicle PBN.

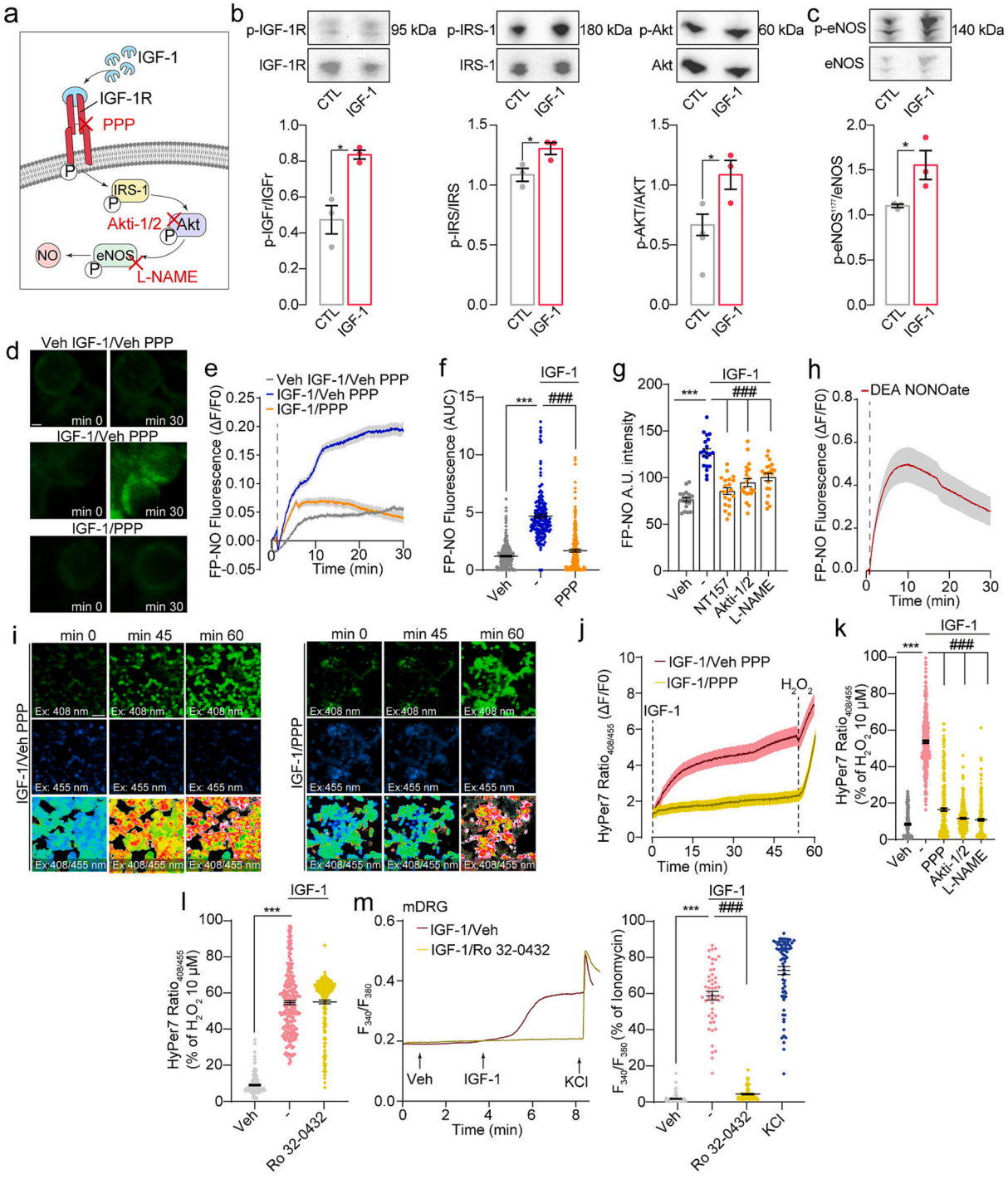

Fig. 4. IGF-1R phosphorylation induces eNOS phosphorylation and NO release (a) Schematic illustration of IGF-1R signaling cascade. (b) Images and cumulative data of non-phosphorylated/phosphorylated ratio of IGF-1R, IRS-1, and Akt in HSCs stimulated with IGF-1/vehicle (n = 3 replicates). (c) Images and cumulative data of non-phosphorylated/phosphorylated ratio of eNOS in HSCs stimulated with IGF-1/vehicle (n = 3 replicates). (d) FP-NO (ΔF/F0) images, (e) traces, and (f) cumulative data of HSCs stimulated with IGF-1/vehicle in the presence of PPP/vehicle (Scale bar: 20 μm) (cells number: IGF-1=207, vehicle = 250, and PPP = 220, n = 3 independent experiments). (g) FP-NO (ΔF/F0) (arbitrary unit, A.U.) cumulative data of HSCs stimulated with IGF-1/vehicle in the presence of NT157, Akt-1/2, or L-NAME/vehicles (n = 20 replicates). (h) FP-NO (ΔF/F0) typical trace of DEA NONOate in HSCs. (i) Images, (j) typical traces, and (k) cumulative data of HyPer7.2, in HSCs, stimulated with IGF-1/vehicle in the presence of PPP, Akti-1/2, or L-NAME/vehicles (Scale bar: 50 μm) (cells number: IGF-1 = 310, vehicles = 237, PPP=280, Akti-1/2 = 227, L-NAME = 236, n = 3 independent experiments). (l) Cumulative data of HyPer7.2 in HSCs stimulated with IGF-1/vehicle in the presence of Ro32-0432/vehicle (cells number: IGF-1 = 244, vehicle = 140, and Ro32-04320 = 232, n = 3 independent experiments). (m) Traces and cumulative data of Ca^{2+} influx (F_{340}/F_{380}) in DRG neurons stimulated with IGF-1/vehicle in the presence of Ro32-0432/vehicle (cells number: IGF-1 = 49, vehicle = 74, Ro32-0432 = 62, and KCl = 74, n = 3 independent experiments). Mean ± SEM. $^{*}P < 0.05$, $^{**}P < 0.01$, $^{***}P < 0.001$ vs. CTL, vehicle; $^{\#\#\#}P < 0.001$ vs. IGF-1/different treatments.

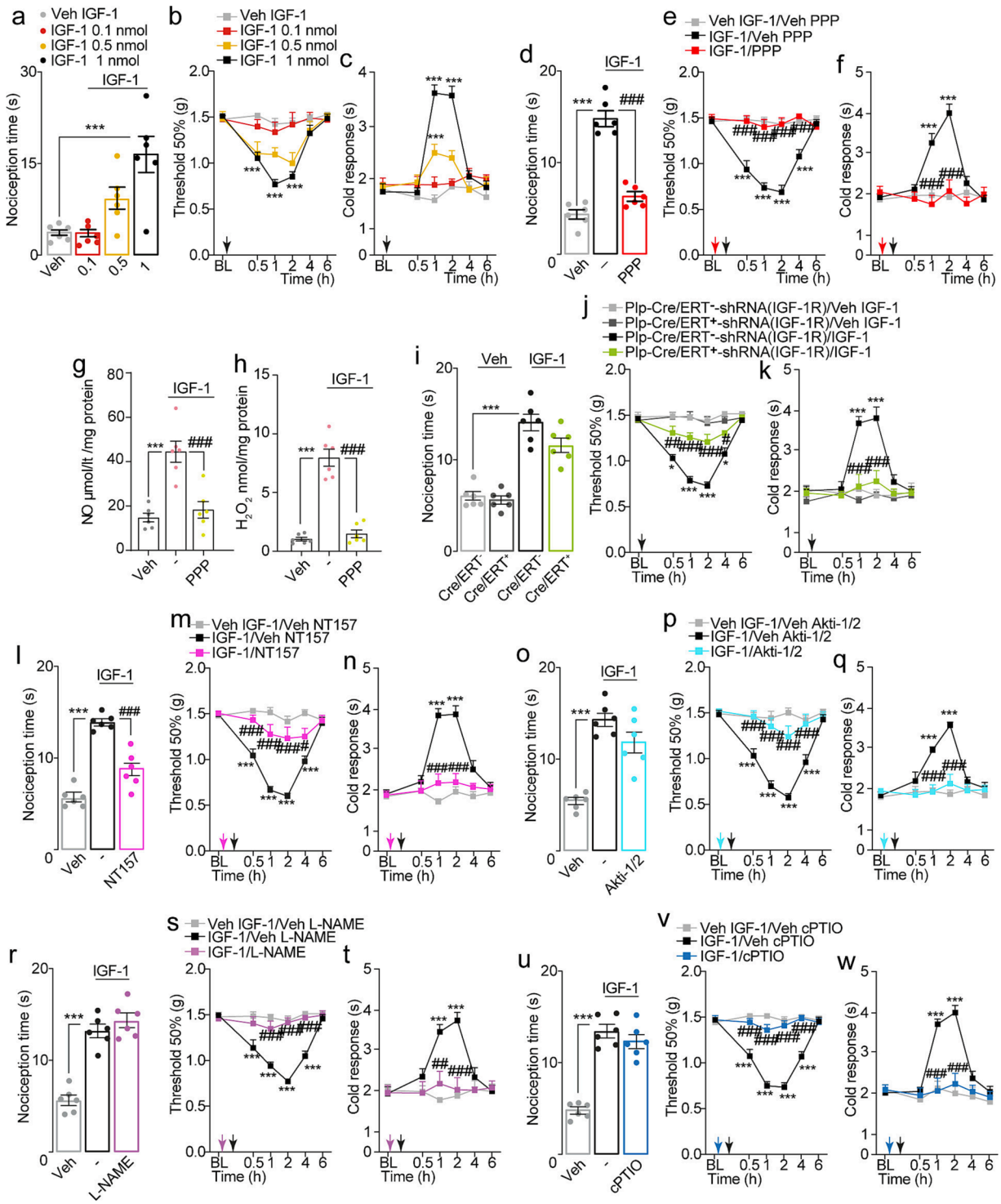

Fig. 5. Schwann cell IGF-1R does not regulate IGF-1 induced acute nociception. Dose- and time-dependent (a) nociceptive response and (b) mechanical/(c) cold allodynia induced by intraplantar (i.pl.) IGF-1/vehicle in C57BL/6J mice. (d) Nociceptive response and (e) mechanical/(f) cold allodynia induced by IGF-1 (1 nMol) /vehicle (i.pl.) in C57BL/6J mice after i.pl. PPP/vehicle (n = 6 mice per group). (g) NO and (h) H_2O_2 content in sciatic nerve tissue homogenates of C57BL/6J mice treated with IGF-1 (1 nMol)/vehicle (i.pl.) and pretreated with PPP/vehicle (i.pl.). (i) Nociceptive response and (j) mechanical/(k) cold allodynia by IGF-1 (1 nMol)/ vehicle (i.pl.) in Plp-Cre/ERT^{-} and Plp-Cre/ERT^{+} infected with AAV-(loxP-shRNA)IGF-1R [E0771/Plp-Cre/ERT^{-}-shRNA(IGF-1R) and E0771/Plp-Cre/ERT^{+}-shRNA (IGF-1R)]. (l, i, r, u) Nociceptive response and (m, p, s, v) mechanical/(n, q, t, w) cold allodynia induced by IGF-1 (1 nMol)/vehicle (i.pl.) in C57BL/6J mice pretreated with NT157 (l–n), Akti-1/2 (o–q), L-NAME (r–t), or cPTIO (u–w) (n = 6 mice per group). Mean ± SEM. (−) represents the combination of various vehicles $^{***}P < 0.001$ vs. vehicle, Cre/ERT^{-}/vehicle, vehicle IGF-1/vehicle NT157, vehicle IGF-1/vehicle Akti-1/2, vehicle IGF-1/vehicle L-NAME, vehicle IGF-1/vehicle cPTIO; $^{\#\#}P < 0.01$, $^{\#\#\#}P < 0.001$ vs. Cre/ERT^{+}/IGF-1, IGF-1/vehicle NT157, IGF-1/vehicle Akti-1/2, IGF-1/vehicle L-NAME, and IGF-1/vehicle cPTIO.

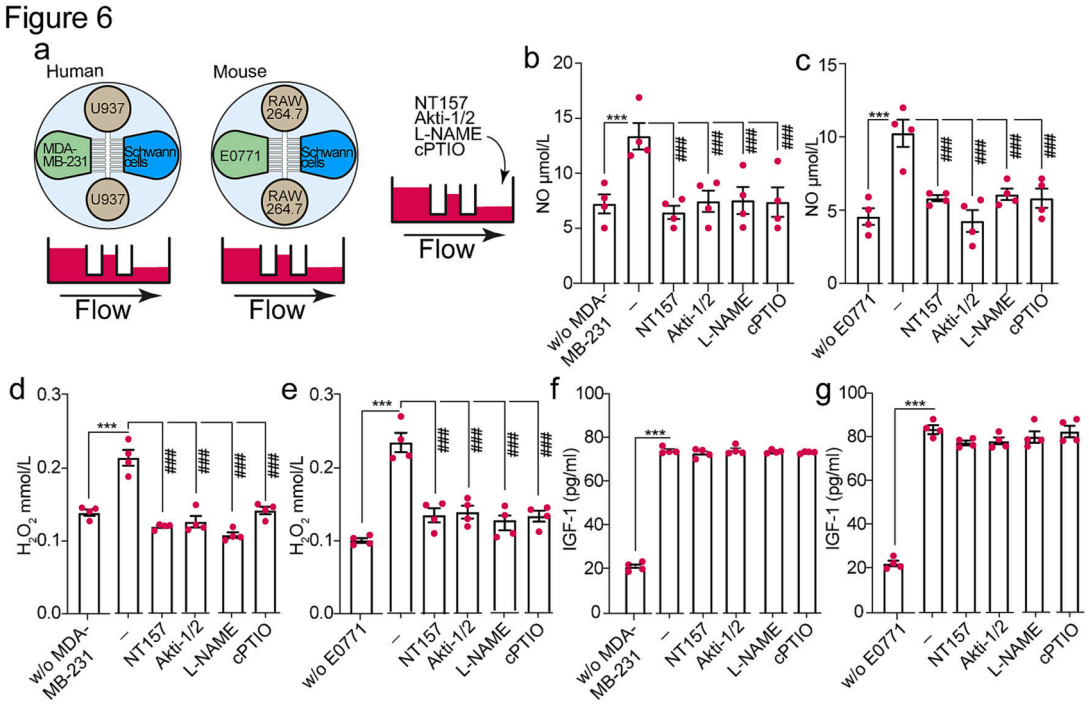

Fig. 6. Osteoclast activation by tumor cells induces NO release by Schwann cells (a) Diagram of the triple co-culture chamber with the mouse (E0771, RAW264.7, and Schwann cells) and human (MDA-MB-231, U937, and Schwann cells). (b, c) NO, (d, e) H_2O_2, and (f, g) IGF-1 levels in human and mouse triple co-culture with or without human or mouse breast cancer cells and in the presence of NT157, Akti-1/2, L-NAME, or cPTIO in HSCs and MSCs chamber (n = 4 replicates). Mean ± SEM. (-) represents the combination of different vehicles, $^{***}P < 0.001$ vs. triple co-culture without cancer cells; $^{###}P < 0.001$ vs. triple co-cultures.

downstream of IGF-1R. *In vivo* studies supported this hypothesis, as mechanical/cold hypersensitivity, but not spontaneous nociception induced by IGF-1 (i.pl.), was attenuated in mice with selective deletion of *Trpa1* in Schwann cells (Plp-Cre/ERT^{+};*Trpa1*$^{fl/fl}$) and in *Trpa1*$^{-/-}$ mice (Fig. 7i–k and Supplementary Fig. 6a–c). Pain-like behaviors observed in control mice were attenuated in Plp-Cre/ERT^{+};*Trpa1*$^{fl/fl}$ and *Trpa1*$^{-/-}$ mice inoculated with E0771 cells (Fig. 7l–o and Supplementary Fig. 6d–g).

3.5. IGF-1 in Schwann cells activates TRPA1 to expand endoneurial macrophages (MΦs)

Recently, in a model of cancer pain, we reported that TRPA1 activation by oxidative stress induced the release of M-CSF from Schwann cells, which expanded endoneurial resident MΦs (rMΦs), thus sustaining mechanical allodynia (De Logu et al., 2021). An increased number of F4/80^{+} (a MΦ biomarker) cells was also observed in the sciatic nerve of E0771-mice (Fig. 8a). To explore the MΦ role in pain-like behaviors, E0771 cells were inoculated in MΦ Fas-Induced Apoptosis (MaFIA) mice, which exhibit a typical and marked reduction in the number of F4/80^{+} cells when injected with the apoptosis inducer, AP20187 (Burnett et al., 2004). E0771 inoculation in MaFIA mice induced tumor growth and pain-like behaviors, like in C57 mice (Fig. 8b–f). AP20187 injections (2 mg/kg, i.p., once a day from day 10 to 20) in E0771-MaFIA mice markedly reduced the increase in sciatic nerve F4/80^{+} cells and pain-like behaviors, but not tumor growth (Fig 8b–g). Then, we investigated whether M-CSF was involved in E0771-evoked MΦ expansion. M-CSF level was increased in sciatic nerve of E0771-mice (Fig. 8h). The M-CSF receptor inhibitor, PLX-3397, attenuated pain-like behaviors, without affecting tumor growth (Fig. 8i–m). In the triple chamber, the absence of cancer cells, osteoclasts, or Schwann cells, or treatment with PPP, PBN, or A967079, reduced M-CSF levels (Fig.8n and o), thus confirming the role of Schwann cell TRPA1 in the cytokine release. It has been reported that activated MΦs release IGF-1, which is implicated in hyperalgesia in a mouse model of endometriosis (Forster et al., 2019). Here, we show that human and murine MΦs (U937 and Raw264.7 cells, respectively) exposed to H_2O_2 release IGF-1 (Fig. 8p and q). MΦ depletion in MaFIA mice significantly attenuated, but did not abolish, IGF-1 levels in sciatic nerve homogenates (Fig. 8r). Osteoclast derived IGF-1 may provide a major contribution to the cancer-dependent proalgesic pathway, including MΦ expansion, but an additional contribution by IGF-1 released from expanded MΦs cannot be excluded.

Finally, the role of neuronal TRPA1 for signaling pain-like behaviors was investigated in E0771 inoculated mice with sensory neuron-specific deletion of TRPA1 (Adv-Cre^{+};*Trpa1*$^{fl/fl}$). In these mice, mechanical/cold hypersensitivity induced by IGF-1 (i.pl.) and pain-like behaviors induced by E0771 cell inoculation were attenuated (Supplementary Fig. 6i–n). In contrast, spontaneous nociceptive behavior induced by IGF-1 (i.pl.), presumably mediated by a direct action on neuronal IGF-1R, was unaffected (Supplementary Fig. 6h), thus confirming the dichotomous proalgesic pathway elicited by i.pl. IGF-1. As previously reported in another model of cancer pain (De Logu et al., 2021), the present results strengthen the hypothesis that Schwann cell TRPA1 activated by IGF-1R amplifies the oxidative stress that sustains pain-like behaviors in the present mouse model of breast cancer cell bone metastases.

4. Discussion

In the present MBCP mouse model, E0771 breast cancer cells inoculated into the mouse mammary gland metastasize to the femur head and, *via* IL-8, subjugate osteoclasts to release osteolytic biomarkers, including IGF-1. The unexpected and major finding of the study is that the entire panel of pain-like behaviors evoked by bone metastasis depends on osteoclast-derived IGF-1, which, targeting the Schwann cell IGF-1R, converts the glial cell into an active proalgesic phenotype. IGF-1R activation in Schwann cells *via* a series of intracellular mediators and TRPA1 releases M-CSF that, promoting endoneurial rMΦs expansion, sustains pain-like behaviors.

Tumor-activated osteoclasts are known to release a series of

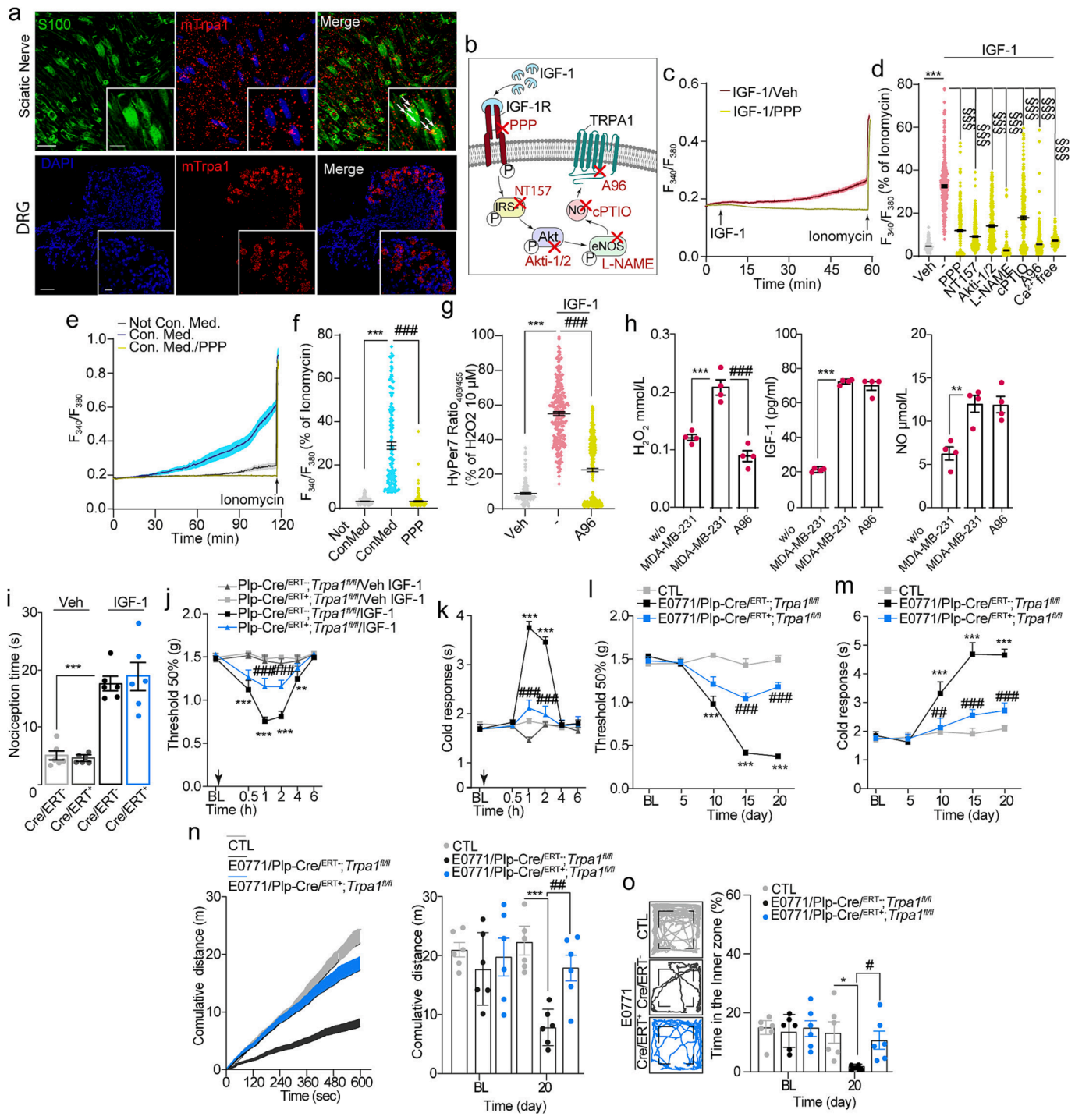

Fig. 7. Schwann cell TRPA1 mediates bone metastatic cancer pain by IGF-1 (a) Images of IGF-1R RNA scope in mouse sciatic nerve and dorsal root ganglia (DRG) (Scale bar: 20 μm, inset 10 μm) (n = 3 subjects). (b) Schematic representation of the TRPA1 activation pathway after IGF-1R activation. (c) Traces and (b) cumulative data of Ca^{2+} influx (F_{340}/F_{380}) in HSCs stimulated with IGF-1/vehicle in Ca^{2+}-free medium (Ca^{2+} free) or in the presence of PPP, NT157, Akt-1/2, L-NAME, cPTIO, or A967079 (A96)/vehicles (cells number: IGF-1=310, vehicles= 233, PPP=344, NT157=348, Akt-1/2=323, L-NAME=316, cPTIO=333, A96=407, and Ca^{2+}free=233, n = 3 independent experiments). (e) Traces and (f) cumulative data of Ca^{2+} influx (F_{340}/F_{380}) in HSCs stimulated with breast cancer cells/osteoclast conditioned medium (ConMed) or normal medium (NotConMed) in the presence of PPP/vehicle (cells number: ConMed=139, NotConMed=166, PPP/vehicle=152, n = 3 independent experiments). (g) HyPer7.2 in HSCs stimulated with IGF-1/vehicle in the presence of A96/vehicle (cells number: IGF-1=234, vehicles=129, A96=316, n = 3 independent experiments). (h) H_2O_2, IGF-1, and NO levels in human triple co-culture (MDA-MB-231, U937 and Schwann cells) and without MDA-MB-231 or in the presence of A96/vehicle in Schwann cells (n = 4 replicates). (i) Nociceptive response and (j) mechanical/(k) cold allodynia induced by IGF-1 (1 nMol)/vehicle (i.pl.) in Plp-Cre/ERT$^-$-*Trpa1*$^{fl/fl}$ Plp-Cre/ERT$^+$-*Trpa1*$^{fl/fl}$ mice. (l) Mechanical (m)/cold allodynia, (n) cumulative distance, and (o) time spent in the inner zone after E0771 cell inoculation in Plp-Cre/ERT$^-$-*Trpa1*$^{fl/fl}$, Plp-Cre/ERT$^+$-*Trpa1*$^{fl/fl}$ or control (CTL) mice (n = 6 mice per group). Mean ± SEM. (-) represents the combination of different vehicles. $^*P < 0.05$, $^{**}P < 0.01$, $^{***}P < 0.001$ vs. vehicle, CTL, NotConMed, Cre/ERT$^-$/vehicle, $^{\#}P < 0.05$, $^{\#\#}P < 0.01$, $^{\#\#\#}P < 0.001$ vs. ConMed, MDA-MB-231, Cre/ERT$^-$/IGF-1, Cre$^-$/IGF-1.

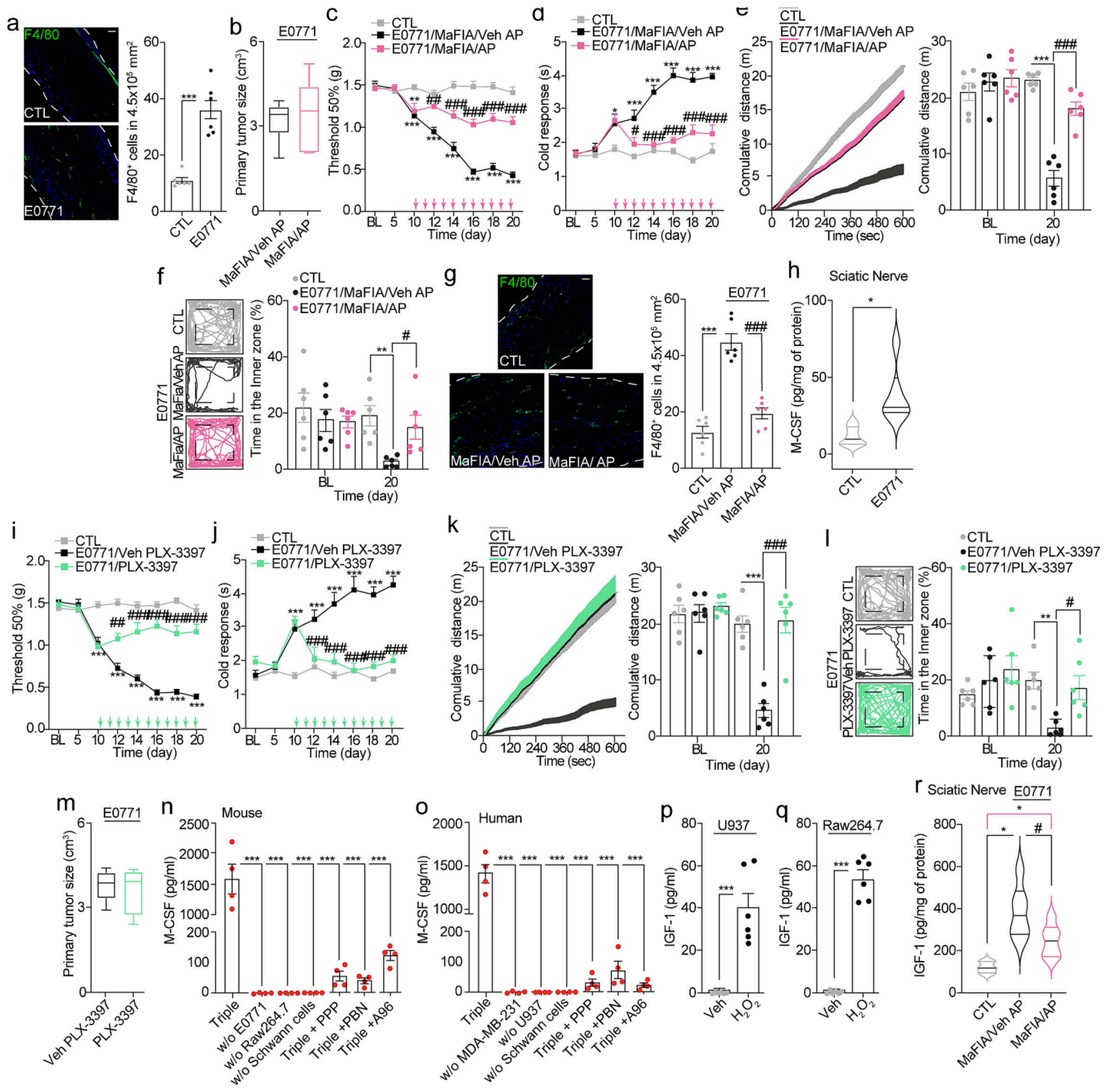

Fig. 8. IGF-1 in Schwann cells activates TRPA1 to expand endoneurial macrophages (MΦs). (a) Number of F4/80$^+$ cells inside the sciatic nerve trunk after E0771 cell inoculation or control (CTL) in C57BL/6J mice (Scale bar: 50 μm) (n = 6 mice per group). (b) Tumor size, (c) mechanical (d)/cold allodynia, (e) cumulative distance (f), and time spent in the inner zone and (g) number of sciatic nerve F4/80$^+$ cells after E0771 cell inoculation in MaFIA/Veh AP, MaFIA/AP or CTL mice. (h) M-CSF levels sciatic nerve tissue homogenates after E0771 cell inoculation or CTL in C57BL/6J mice (Scale bar: 50 μm) (n = 6 mice per group). (i) Mechanical (j)/cold allodynia, (k) cumulative distance, (l) time spent in the inner zone, and (m) primary tumor size after E0771 cell inoculation or CTL in C57BL/6J mice treated with PLX-3397/vehicle (i.p.) (n = 6 mice per group). (n-o) M-CSF levels in human and mouse triple co-culture with or without osteoclasts, cancer cells and Schwann cells, or in the presence of PPP, PBN or A967079 (A96) in Schwann cells (n = 4 replicates). (p–q) IGF-1 levels in human and mouse MΦs (U937 and Raw264.7 cells respectively) exposed to H_2O_2 (100 mM) or vehicle (Veh). (r) IGF-1 levels in sciatic nerve tissue homogenates after E0771 cell inoculation in MaFIA/Veh AP, MaFIA/AP or CTL mice (n = 6 mice per group). Mean ± SEM. $^*P < 0.05$, $^{**}P < 0.01$, $^{***}P < 0.001$ vs. CTL, Veh $^{\#}P < 0.05$, $^{\#\#}P < 0.01$, $^{\#\#\#}P < 0.001$ vs. E0771/MaFIA/Veh AP, E0771/Veh PLX-3397, MaFIA/Veh AP.

osteolytic biomarkers, including TGF-β, IL-6, and IGF-1 (Breuksch et al., 2016; Chen et al., 2010; Hiraga et al., 2012). Results obtained with inhibition of IGF-1 signaling by an IGF-1R antagonist and anti-IGF-1 neutralizing antibodies disclosed the critical role of IGF-1 in generating pain-like behaviors. IGF-1 has been implicated in various mouse pain models, including chronic constriction injury (Chen et al., 2021), carrageenan-induced inflammation (Manzano-Garcia and Gamal-Eltrabily, 2017), and type 2 diabetic neuropathy (Tang et al., 2019). Although previous (Bitar et al., 1996; Bonnefont et al., 2007) and recent (Kohno et al., 2022) studies have suggested that IGF-1 exerts analgesic effects in the CNS, general consensus indicates that its peripheral administration elicits acute nociceptive response and prolonged

mechanical and thermal hypersensitivity (Tang et al., 2019; Zhang et al., 2014). This conclusion is strengthened by present observations that perineural, but not central, administration of a neutralizing antibody against IGF-1 reverted pain-like behaviors, thus excluding the contribution of central IGF-1 in our model of MBCP.

The proalgesic effects of IGF-1 peripheral administration have been ascribed to a direct action on IGF-1R expressed by DRG neurons (Zhang et al., 2014). The present data obtained by IGF-1R cell-selective silencing confirm the role of neuronal IGF-1R in acute nociception. However, they reveal an unforeseen role of Schwann cell IGF-1R in sustaining mechanical/cold hypersensitivity evoked by i.pl. IGF-1 injection, thus highlighting a dichotomous action of IGF-1 in DRG neurons and peripheral glial cells. IGF-1 injection (i.pl.) elicits two distinct types of responses: an early and transient acute nociception and a delayed and persistent mechanical/cold hypersensitivity. Silencing of IGF-1R in DRG neurons attenuated acute nociception, leaving sustained mechanical/cold hypersensitivity unaffected. *Vice versa*, silencing IGF-1R in Schwann cells inhibited mechanical/cold hypersensitivity without affecting acute nociception. These findings have major pathophysiological consequences as selective silencing of IGF-1R in DRG neurons failed to attenuate pain-like behaviors evoked by E0771 cell inoculation, which, in contrast, were inhibited in mice with selective silencing of IGF-1R in Schwann cells.

IGF binding proteins (IGFBPs) can affect the extent of IGF-1 signaling (Zhou et al., 2003). In particular, the interaction of IGFBP-4, which is abundantly expressed in bone tissue, with IGF-1, has been shown to prevent IGF-1R activation (Mohan et al., 1995; Schiltz et al., 1993). However, there is no evidence that increased levels of IGFBP-4, or other IGFBPs modulating IGF-1R signaling, reduce MBCP. Some promiscuity in IGF-1R signaling has been reported. In fact, IGF-2 and insulin have been shown to promote the same intracellular pathway, *via* the activation of hybrid receptors *via* insulin half receptors (Benyoucef et al., 2007). However, if and how this non-canonical signaling pathway might trigger a response implicated in the Schwann cell algesic pathway is currently unknown.

The divergent proalgesic responses to IGF-1 in DRG neurons and Schwann cells are encoded by distinct intracellular pathways recruited by IGF-1R activation in the two cell types (Supplementary Fig. 7) IGF-1R activation in cultured mouse DRG neurons promotes a PKCα-dependent T-type channel Ca^{2+} influx, which has been associated with peripheral pain (Zhang et al., 2014). However, the PKC inhibitor, Ro32-0432, attenuated acute nociception but failed to inhibit prolonged mechanical/cold hypersensitivity evoked by i.pl. IGF-1 injection. In Schwann cells, IGF-1R trans-phosphorylation did not activate PKC, but stimulated IRS-1 and the AKT-dependent cascade that promotes eNOS phosphorylation. Activated IRS-1 interacts with the clathrin adaptor protein complex (AP2) to prevent IGF-1R clathrin-mediated endocytosis, thereby prolonging receptor activity (Yoneyama et al., 2018). Here, we show that an IRS-1 inhibitor (NT157) prevented mechanical/cold hypersensitivity induced by i.pl. IGF-1 injection. Notably, mechanical/cold hypersensitivity and pain-like behaviors were not apparently due to endosome internalization, as the combination of an IRS-1 inhibitor and a clathrin-mediated endocytosis inhibitor (PitStop2) failed to restore sustained mechanical/cold hypersensitivity and pain-like behaviors. In contrast, acute nociception produced by i.pl. IGF-1 injection, reduced by IRS-1 inhibition, was restored by the clathrin inhibitor, thus supporting the existence of two distinct and cell-specific IGF-1 signaling pathways. In DRG neurons, permanence of IGF-1R to the plasma membrane mediated by IRS-1 and PKC activation encodes the acute nociception response induced by IGF-1, attenuated by the clathrin-dependent internalization. In contrast, IRS-1 elicits sustained mechanical/cold hypersensitivity *via* a different pathway in Schwann cells, which is independent of PKC and clathrin-mediated endocytosis, is mediated by eNOS phosphorylation, and is the sole mechanism implicated in pain-like behaviors observed in the current model of MBCP.

IGF-1 stimulation of cultured Schwann cells resulted in eNOS phosphorylation and the ensuing NO release. Inoculation of osteosarcoma cells in the femurs of C3H/HeJ mice induces pain-like behaviors through the activation of neuronal and inducible NOS isoforms (nNOS and iNOS, respectively) in the spinal cord (Yang et al., 2016). Here, we show that administration of the NO scavenger, cPTIO, or the NOS inhibitor, L-NAME, attenuated pain-like behaviors in mice inoculated with E0771 cells and sustained mechanical/cold hypersensitivity elicited by i.pl. IGF-1. Failure of cPTIO and L-NAME to reduce acute nociception induced by i.pl. IGF-1 strengthens the hypothesis that NO released by Schwann cell eNOS is necessary and sufficient for generating prolonged proalgesic responses, including mechanical/cold hypersensitivity by IGF-1 and cancer-evoked pain-like behaviors, as previously proposed in a model of CGRP-evoked periorbital mechanical allodynia (De Logu et al., 2022).

Inoculation of melanoma cancer cells in mouse hind paw was shown to cause M-CSF release from Schwann cells, which promotes the expansion of endoneurial rMΦs (De Logu et al., 2021). The resulting oxidative stress targets neuronal TRPA1 to signal mechanical hypersensitivity (De Logu et al., 2021). In the present MBCP model, E0771 breast carcinoma cells growing in the femur metastasis release IL-8, which stimulates osteoclasts to liberate IGF-1. The ensuing IGF-1R activation in Schwann cells results in NO production that targets Schwann cell TRPA1. Activated TRPA1 releases M-CSF that promotes endoneurial rMΦ expansion and the ensuing ROS generation sustains mechanical allodynia by targeting neuronal TRPA1. Therefore, we propose that the humoral communication between osteoclasts and Schwann cells converges in a final common pathway implicating a role of NO/TRPA1/oxidative stress that is observed in different mouse models of cancer or neuropathic pain. However, this conclusion does not implicate that different proalgesic pathways contribute to MBCP. Glial cell-selective targeting of the various mediators that sustain proalgesic signals initiated by Schwann cell IGF-1R activation could be a promising area for future treatments against MBCP.

Funding

This study was supported by grants from the Associazione Italiana per la Ricerca sul Cancro (AIRC) under IG 2020-ID 24503 (RN), Finanziamento di progetti competitivi per Ricercatori a Tempo Determinato, University of Florence 2020-2021 (RN, FB), and the European Research Council (ERC) under the European Union's Horizon 2020 Research and Innovation Programme (grant agreement No. 835286) (PG).

Data and materials availability

All data associated with this study are presented in the paper or the Supplementary Materials. The materials generated from this study are available upon request from Romina Nassini (romina.nassini@unifi.it).

Declaration of Competing Interest

The authors declare the following financial interests/personal relationships which may be considered as potential competing interests: FDL, PG, and RN are the founding scientists of FloNext Srl. PG has been in advisory boards and/or received fees for lectures from Novartis, Amgen, TEVA, AbbVie, Eli-Lilly, Lundbeck. The other authors have no conflicts of interest to declare.

Data availability

Data will be made available on request.

Acknowledgments

We would like to thank Editage (www.editage.com) for English language editing.

Appendix A. Supplementary data

Supplementary data to this article can be found online at https://doi.org/10.1016/j.bbi.2023.03.013.

References

Aielli, F., Ponzetti, M., Rucci, N., 2019. Bone Metastasis Pain, from the Bench to the Bedside. Int. J. Mol. Sci. 20.

Amoui, M., Suhr, S.M., Baylink, D.J., Lau, K.H., 2004. An osteoclastic protein-tyrosine phosphatase may play a role in differentiation and activity of human monocytic U-937 cell-derived, osteoclast-like cells. Am J Physiol Cell Physiol 287, C874-884.

Andriessen, A.S., Donnelly, C.R., Ji, R.R., 2021. Reciprocal interactions between osteoclasts and nociceptive sensory neurons in bone cancer pain. Pain Rep 6, e867.

Antoniazzi, C.T.D., Nassini, R., Rigo, F.K., Milioli, A.M., Bellinaso, F., Camponogara, C., Silva, C.R., de Almeida, A.S., Rossato, M.F., De Logu, F., Oliveira, S.M., Cunha, T.M., Geppetti, P., Ferreira, J., Trevisan, G., 2019. Transient receptor potential ankyrin 1 (TRPA1) plays a critical role in a mouse model of cancer pain. Int. J. Cancer 144, 355–365.

Ara, T., Declerck, Y.A., 2010. Interleukin-6 in bone metastasis and cancer progression. Eur. J. Cancer 46, 1223–1231.

Aukes, K., Forsman, C., Brady, N.J., Astleford, K., Blixt, N., Sachdev, D., Jensen, E.D., Mansky, K.C., Schwertfeger, K.L., 2017. Breast cancer cell-derived fibroblast growth factors enhance osteoclast activity and contribute to the formation of metastatic lesions. PLoS One 12, e0185736.

Benyoucef, S., Surinya, K.H., Hadaschik, D., Siddle, K., 2007. Characterization of insulin/IGF hybrid receptors: contributions of the insulin receptor L2 and Fn1 domains and the alternatively spliced exon 11 sequence to ligand binding and receptor activation. Biochem. J 403, 603–613.

Bitar, M.S., Al-Bustan, M., Nehme, C.L., Pilcher, C.W., 1996. Antinociceptive action of intrathecally administered IGF-I and the expression of its receptor in rat spinal cord. Brain Res. 737, 292–294.

Bonnefont, J., Daulhac, L., Etienne, M., Chapuy, E., Mallet, C., Ouchchane, L., Deval, C., Courade, J.P., Ferrara, M., Eschalier, A., Clottes, E., 2007. Acetaminophen recruits spinal p42/p44 MAPKs and GH/IGF-1 receptors to produce analgesia via the serotonergic system. Mol. Pharmacol. 71, 407–415.

Breuksch, I., Weinert, M., Brenner, W., 2016. The role of extracellular calcium in bone metastasis. J Bone Oncol 5, 143–145.

Burnett, S.H., Kershen, E.J., Zhang, J., Zeng, L., Straley, S.C., Kaplan, A.M., Cohen, D.A., 2004. Conditional macrophage ablation in transgenic mice expressing a Fas-based suicide gene. J. Leukoc. Biol. 75, 612–623.

Chaplan, S.R., Bach, F.W., Pogrel, J.W., Chung, J.M., Yaksh, T.L., 1994. Quantitative assessment of tactile allodynia in the rat paw. J. Neurosci. Methods 53, 55–63.

Chen, X., Le, Y., He, W.Y., He, J., Wang, Y.H., Zhang, L., Xiong, Q.M., Zheng, X.Q., Liu, K. X., Wang, H.B., 2021. Abnormal Insulin-like Growth Factor 1 Signaling Regulates Neuropathic Pain by Mediating the Mechanistic Target of Rapamycin-Related Autophagy and Neuroinflammation in Mice. ACS Chem. Nerosci. 12, 2917–2928.

Chen, Y.C., Sosnoski, D.M., Mastro, A.M., 2010. Breast cancer metastasis to the bone: mechanisms of bone loss. Breast Cancer Res. 12, 215.

Dam, D.H.M., Jelsma, S.A., Yu, J.M., Liu, H., Kong, B., Paller, A.S., 2020. Flotillin and AP2A1/2 Promote IGF-1 Receptor Association with Clathrin and Internalization in Primary Human Keratinocytes. J, Invest. Dermatol. 140 (1743–1752), e1744.

De Logu, F., Nassini, R., Materazzi, S., Carvalho Goncalves, M., Nosi, D., Rossi Degl'Innocenti, D., Marone, I.M., Ferreira, J., Li Puma, S., Benemei, S., Trevisan, G., Monteiro, S., de Araujo, D., Patacchini, R., Bunnett, N.W., Geppetti, P., 2017. Schwann cell TRPA1 mediates neuroinflammation that sustains macrophage-dependent neuropathic pain in mice. Nat. Commun. 8, 1887.

De Logu, F., Li Puma, S., Landini, L., Portelli, F., Innocenti, A., de Araujo, D.S.M., Janal, M.N., Patacchini, R., Bunnett, N.W., Geppetti, P., Nassini, R., 2019. Schwann cells expressing nociceptive channel TRPA1 orchestrate ethanol-evoked neuropathic pain in mice. J. Clin. Invest. 129, 5424–5441.

De Logu, F., Marini, M., Landini, L., Monteiro, S., de Araujo, D., Bartalucci, N., Trevisan, G., Bruno, G., Marangoni, M., Schmidt, B.L., Bunnett, N.W., Geppetti, P., Nassini, R., 2021. Peripheral Nerve Resident Macrophages and Schwann Cells Mediate Cancer-Induced Pain. Cancer Res. 81, 3387–3401.

De Logu, F., Nassini, R., Hegron, A., Landini, L., Jensen, D.D., Latorre, R., Ding, J., Marini, M., Monteiro, S., de Araujo, D., Ramirez-Garcia, P., Whittaker, M., Retamal, J., Titiz, M., Innocenti, A., Davis, T.P., Veldhuis, N., Schmidt, B.L., Bunnett, N.W., Geppetti, P., 2022. Schwann cell endosome CGRP signals elicit periorbital mechanical allodynia in mice. Nat. Commun. 13, 646.

Deuis, J.R., Dvorakova, L.S., Vetter, I., 2017. Methods Used to Evaluate Pain Behaviors in Rodents. Front. Mol. Neurosci. 10, 284.

Eberhardt, M., Dux, M., Namer, B., Miljkovic, J., Cordasic, N., Will, C., Kichko, T.I., de la Roche, J., Fischer, M., Suarez, S.A., Bikiel, D., Dorsch, K., Leffler, A., Babes, A., Lampert, A., Lennerz, J.K., Jacobi, J., Marti, M.A., Doctorovich, F., Hogestatt, E.D., Zygmunt, P.M., Ivanovic-Burmazovic, I., Messlinger, K., Reeh, P., Filipovic, M.R., 2014. H2S and NO cooperatively regulate vascular tone by activating a neuroendocrine HNO-TRPA1-CGRP signalling pathway. Nat. Commun. 5, 4381.

Echeverry, S., Shi, X.Q., Haw, A., Liu, H., Zhang, Z.W., Zhang, J., 2009. Transforming growth factor-beta1 impairs neuropathic pain through pleiotropic effects. Mol. Pain 5, 16.

Ewens, A., Mihich, E., Ehrke, M.J., 2005. Distant metastasis from subcutaneously grown E0771 medullary breast adenocarcinoma. Anticancer Res 25, 3905–3915.

Faul, F., Erdfelder, E., Lang, A.G., Buchner, A., 2007. G*Power 3: a flexible statistical power analysis program for the social, behavioral, and biomedical sciences. Behav. Res. Methods 39, 175–191.

Fohr, B., Dunstan, C.R., Seibel, M.J., 2003. Clinical review 165: Markers of bone remodeling in metastatic bone disease. J. Clin. Endocrinol. Metab. 88, 5059–5075.

Forouzanfar, F., Sadeghnia, H.R., 2020. Fibroblast Growth Factors as Tools in the Management of Neuropathic Pain Disorders. Curr. Drug Targets 21, 1034–1043.

Forster, R., Sarginson, A., Velichkova, A., Hogg, C., Dorning, A., Horne, A.W., Saunders, P.T.K., Greaves, E., 2019. Macrophage-derived insulin-like growth factor-1 is a key neurotrophic and nerve-sensitizing factor in pain associated with endometriosis. FASEB J. 33, 11210–11222.

Guise, T.A., 2000. Molecular mechanisms of osteolytic bone metastases. Cancer 88, 2892–2898.

Han, Q., Liu, J., Meng, Q., Wang, Y.L., Feng, H., Zhang, Z., Xu, Z.P., Zhang, R., 2019. Turn-On Fluorescence Probe for Nitric Oxide Detection and Bioimaging in Live Cells and Zebrafish. ACS Sens 4, 309–316.

Hiraga, T., Myoui, A., Hashimoto, N., Sasaki, A., Hata, K., Morita, Y., Yoshikawa, H., Rosen, C.J., Mundy, G.R., Yoneda, T., 2012. Bone-derived IGF mediates crosstalk between bone and breast cancer cells in bony metastases. Cancer Res. 72, 4238–4249.

Hiraga, T., Ninomiya, T., 2019. Establishment and characterization of a C57BL/6 mouse model of bone metastasis of breast cancer. J. Bone Miner. Metab. 37, 235–242.

Huang, W., Calvo, M., Karu, K., Olausen, H.R., Bathgate, G., Okuse, K., Bennett, D.L.H., Rice, A.S.C., 2013. A clinically relevant rodent model of the HIV antiretroviral drug stavudine induced painful peripheral neuropathy. Pain 154, 560–575.

Islam, S., Hassan, F., Tumurkhuu, G., Dagvadorj, J., Koide, N., Naiki, Y., Mori, I., Yoshida, T., Yokochi, T., 2007. Bacterial lipopolysaccharide induces osteoclast formation in RAW 264.7 macrophage cells. Biochem. Biophys. Res. Commun. 360, 346–351.

Katsuno, Y., Hanyu, A., Kanda, H., Ishikawa, Y., Akiyama, F., Iwase, T., Ogata, E., Ehata, S., Miyazono, K., Imamura, T., 2008. Bone morphogenetic protein signaling enhances invasion and bone metastasis of breast cancer cells through Smad pathway. Oncogene 27, 6322–6333.

Kavran, J.M., McCabe, J.M., Byrne, P.O., Connacher, M.K., Wang, Z., Ramek, A., Sarabipour, S., Shan, Y., Shaw, D.E., Hristova, K., Cole, P.A., Leahy, D.J., 2014. How IGF-1 activates its receptor. Elife 3.

Kohno, K., Shirasaka, R., Yoshihara, K., Mikuriya, S., Tanaka, K., Takanami, K., Inoue, K., Sakamoto, H., Ohkawa, Y., Masuda, T., Tsuda, M., 2022. A spinal microglia population involved in remitting and relapsing neuropathic pain. Science 376, 86–90.

Kwan, K.Y., Allchorne, A.J., Vollrath, M.A., Christensen, A.P., Zhang, D.S., Woolf, C.J., Corey, D.P., 2006. TRPA1 contributes to cold, mechanical, and chemical nociception but is not essential for hair-cell transduction. Neuron 50, 277–289.

Le Pape, F., Vargas, G., Clézardin, P., 2016. The role of osteoclasts in breast cancer bone metastasis. J Bone Oncol 5, 93–95.

Li, Y., Cai, J., Han, Y., Xiao, X., Meng, X.L., Su, L., Liu, F.Y., Xing, G.G., Wan, Y., 2014. Enhanced function of TRPV1 via up-regulation by insulin-like growth factor-1 in a rat model of bone cancer pain. Eur. J. Pain 18, 774–784.

Long, L., Wu, Y., Wang, L., Gong, A., Hu, F., Zhang, C., 2015. A fluorescent probe for hypochlorite based on the modulation of the unique rotation of the N-N single bond in acetohydrazide. Chem. Commun. (Camb) 51, 10435–10438.

Mantyh, P., 2006. The science behind metastatic bone pain. Eur. J. Cancer Suppl. 4, 4–8.

Mantyh, P.W., 2014. Bone cancer pain: from mechanism to therapy. Curr. Opin. Support. Palliat. Care 8, 83–90.

Manzano-Garcia, A., Gamal-Eltrabily, M., 2017. A new role of growth hormone and insulin growth factor receptor type 1 in neonatal inflammatory nociception. Pain Rep 2, e608.

McGrath, J.C., Lilley, E., 2015. Implementing guidelines on reporting research using animals (ARRIVE etc.): new requirements for publication in BJP. Br. J. Pharmacol. 172, 3189–3193.

Mitchell, K., Shah, J.P., Dalgard, C.L., Tsytsikova, L.V., Tipton, A.C., Dmitriev, A.E., Symes, A.J., 2016. Bone morphogenetic protein-2-mediated pain and inflammation in a rat model of posterolateral arthrodesis. BMC Neurosci. 17, 80.

Miura, M., Sasaki, M., Mizukoshi, K., Shibasaki, M., Izumi, Y., Shimosato, G., Amaya, F., 2011. Peripheral sensitization caused by insulin-like growth factor 1 contributes to pain hypersensitivity after tissue injury. Pain 152, 888–895.

Mohan, S., Nakao, Y., Honda, Y., Landale, E., Leser, U., Dony, C., Lang, K., Baylink, D.J., 1995. Studies on the mechanisms by which insulin-like growth factor (IGF) binding protein-4 (IGFBP-4) and IGFBP-5 modulate IGF actions in bone cells. J. Biol. Chem. 270, 20424–20431.

Nachat-Kappes, R., Pinel, A., Combe, K., Lamas, B., Farges, M.C., Rossary, A., Goncalves-Mendes, N., Caldefie-Chezet, F., Vasson, M.P., Basu, S., 2012. Effects of enriched environment on COX-2, leptin and eicosanoids in a mouse model of breast cancer. PLoS One 7, e51525.

Nicolson, G.L., Brunson, K.W., Fidler, I.J., 1978. Specificity of arrest, survival, and growth of selected metastatic variant cell lines. Cancer Res. 38, 4105–4111.

Pak, V.V., Ezeriņa, D., Lyublinskaya, O.G., Pedre, B., Tyurin-Kuzmin, P.A., Mishina, N. M., Thauvin, M., Young, D., Wahni, K., Martínez Gache, S.A., Demidovich, A.D., Ermakova, Y.G., Maslova, Y.D., Shokhina, A.G., Eroglu, E., Bilan, D.S., Bogeski, I., Michel, T., Vriz, S., Messens, J., Belousov, V.V., 2020. Ultrasensitive Genetically Encoded Indicator for Hydrogen Peroxide Identifies Roles for the Oxidant in Cell Migration and Mitochondrial Function. Cell Metab. 31, 642–653.e646.

Rades, D., Schild, S.E., Abrahm, J.L., 2010. Treatment of painful bone metastases. Nat. Rev. Clin. Oncol. 7, 220–229.

Schiltz, P.M., Mohan, S., Baylink, D.J., 1993. Insulin-like growth factor binding protein-4 inhibits both basal and IGF-mediated chick pelvic cartilage growth in vitro. J. Bone Miner. Res. 8, 391–396.
Schnütgen, F., Doerflinger, N., Calléja, C., Wendling, O., Chambon, P., Ghyselinck, N.B., 2003. A directional strategy for monitoring Cre-mediated recombination at the cellular level in the mouse. Nat. Biotechnol. 21, 562–565.
Sugawara, S., Shinoda, M., Hayashi, Y., Saito, H., Asano, S., Kubo, A., Shibuta, I., Furukawa, A., Toyofuku, A., Iwata, K., 2019. Increase in IGF-1 Expression in the Injured Infraorbital Nerve and Possible Implications for Orofacial Neuropathic Pain. Int. J. Mol. Sci. 20.
Syroid, D.E., Zorick, T.S., Arbet-Engels, C., Kilpatrick, T.J., Eckhart, W., Lemke, G., 1999. A role for insulin-like growth factor-I in the regulation of Schwann cell survival. J. Neurosci. 19, 2059–2068.
Takayama, B., Sekiguchi, M., Yabuki, S., Kikuchi, S., Konno, S., 2011. Localization and function of insulin-like growth factor 1 in dorsal root ganglia in a rat disc herniation model. Spine (Phila Pa 1976) 36, E75-79.
Tang, Z., Cao, F., Zhang, H., Tang, J., Li, H., Zhang, Y., Feng, B., Wang, H., 2019. Peripheral pain is enhanced by insulin-like growth factor 1 and its receptors in a mouse model of type 2 diabetes mellitus. J. Diabetes 11, 309–315.
von Moos, R., Costa, L., Ripamonti, C.I., Niepel, D., Santini, D., 2017. Improving quality of life in patients with advanced cancer: Targeting metastatic bone pain. Eur. J. Cancer 71, 80–94.
Wang, Q., Li, H.Y., Ling, Z.M., Chen, G., Wei, Z.Y., 2022. Inhibition of Schwann cell pannexin 1 attenuates neuropathic pain through the suppression of inflammatory responses. J. Neuroinflammation 19, 244.
Weilbaecher, K.N., Guise, T.A., McCauley, L.K., 2011. Cancer to bone: a fatal attraction. Nat. Rev. Cancer 11, 411–425.
Yang, Y., Zhang, J., Liu, Y., Zheng, Y., Bo, J., Zhou, X., Wang, J., Ma, Z., 2016. Role of nitric oxide synthase in the development of bone cancer pain and effect of L-NMMA. Mol. Med. Rep. 13, 1220–1226.
Yoneyama, Y., Lanzerstorfer, P., Niwa, H., Umehara, T., Shibano, T., Yokoyama, S., Chida, K., Weghuber, J., Hakuno, F., Takahashi, S.I., 2018. IRS-1 acts as an endocytic regulator of IGF-I receptor to facilitate sustained IGF signaling. Elife 7.
Zajaczkowska, R., Kocot-Kepska, M., Leppert, W., Wordliczek, J., 2019. Bone Pain in Cancer Patients: Mechanisms and Current Treatment. Int J Mol Sci 20.
Zhang, C., Li, H., Han, R., 2020. An open-source video tracking system for mouse locomotor activity analysis. BMC. Res. Notes 13, 48.
Zhang, Y., Qin, W., Qian, Z., Liu, X., Wang, H., Gong, S., Sun, Y.G., Snutch, T.P., Jiang, X., Tao, J., 2014. Peripheral pain is enhanced by insulin-like growth factor 1 through a G protein-mediated stimulation of T-type calcium channels. Sci. Signal. 7, ra94.
Zhou, R., Diehl, D., Hoeflich, A., Lahm, H., Wolf, E., 2003. IGF-binding protein-4: biochemical characteristics and functional consequences. J. Endocrinol. 178, 177–193.
Zhou, Y.Q., Liu, Z., Liu, Z.H., Chen, S.P., Li, M., Shahveranov, A., Ye, D.W., Tian, Y.K., 2016. Interleukin-6: an emerging regulator of pathological pain. J. Neuroinflammation 13, 141.
Zurborg, S., Piszczek, A., Martinez, C., Hublitz, P., Al Banchaabouchi, M., Moreira, P., Perlas, E., Heppenstall, P.A., 2011. Generation and characterization of an Advillin-Cre driver mouse line. Mol. Pain 7, 66.